M.R P. 1018
S.C. 11/222
7th December, 1956

METEOROLOGICAL OFFICE
17 JUN 1957
LIBRARY

Numerical experiments in the integration of the meteorological equations of motion

by

E. Knighting, D. E. Jones and Mavis K. Hinds

(Meteorological Office)

AIR MINISTRY

METEOROLOGICAL RESEARCH COMMITTEE

FG1A

At the time of issue this report has not been published. Any author desiring to quote this paper should refer to it as "A paper of the Meteorological Research Committee (London), M.R.P. No. 1018 by E. Knighting, D.E. Jones and Mavis K. Hinds. A copy is available in the Library of the Meteorological Office."

M.R.P. 1018
S.C.II/222
7th December, 1956

AIR MINISTRY

METEOROLOGICAL RESEARCH COMMITTEE

Numerical experiments in the integration of the meteorological equations of motion

by

E. Knighting, D.E. Jones and Mavis K. Hinds (Meteorological Office)

Summary

It is usual to use finite difference methods in carrying out the time integration of the equations of motion as adapted to the prediction of the large scale atmospheric pattern, and this implies a choice of the mesh length and time increment to be used. The effect of changing the size and orientation of the mesh upon the computed values of the vorticities and their advection is examined, and the resulting differences between 24-hour predictions are shown to be important.

1. Introduction

The so-called "vorticity equation" relating changes of the vertical component of vorticity to the advection and divergence forms the basis of all practical methods of numerical weather prediction so far developed. In particular the barotropic equation used in the simplest system of practical value is merely an expression of the conservation of absolute vorticity.

Hence in the numerical calculations involved in predicting the synoptic-scale flow pattern over a period of a day or so we have to deal with expressions of the form

$$\frac{\partial \zeta}{\partial t} + \mathbf{V} \cdot \nabla \zeta$$

where ζ is the vertical component of vorticity. Further it has been found necessary to make use of the quasi-geostrophic character of the motion and assume that the velocity, but not its divergence, can be derived from the geopotential

$$\mathbf{V} = \frac{g}{f} \mathbf{k} \wedge \nabla h \qquad \ldots\ldots\ldots(1)$$

where $\mathbf{V}$ is the velocity, h the height of an isobaric surface, g the acceleration due to gravity and f the Coriolis parameter; the gradient is taken in the isobaric surface. The vorticity ζ, is then given by

$$\zeta = \frac{g}{f} \nabla^2 h \qquad \ldots\ldots\ldots(2)$$

/The

The term $\mathbf{V}.\nabla\zeta$ may be written, in view of equation (1) as

$$\mathbf{V}.\nabla\zeta = \frac{g}{f} J(h,\zeta) \qquad \ldots\ldots\ldots(3)$$

J denoting, as usual, the Jacobian so that the typical equation with which we deal is

$$\nabla^2 \frac{\partial h}{\partial t} + J(h,\zeta) = F(h,\zeta,f) \qquad \ldots\ldots\ldots(4)$$

Explicit solutions of such equations cannot be obtained and the integration is carried out by replacing the equations by their finite difference analogues in terms of the height of a pressure surface (or the thickness between two pressure surfaces) at the grid points of a square mesh. The initial values of h at the grid points are not observed but are interpolated and even extrapolated values obtained from observations which are irregularly distributed. The finite difference approximations to ∇^2 and J will depend upon both the length and orientation of the mesh, although the differential operators themselves are symmetrical. The object of this investigation is to compare the finite difference approximations to ∇^2 and J using different mesh lengths and orientations and to find their effect upon the time integrations.

2. The basis of the computations

One finite difference approximation to $\nabla^2 h$ is

$$\nabla^2 h = \frac{h_1 + h_2 + h_3 + h_4 - 4h_0}{a^2} \qquad \ldots\ldots\ldots(5)$$

where the symbol ∇^2 indicates a finite difference approximation, and h_i is the value of h at the grid point numbered i in Fig.1, a being the mesh length. A similar formula applies if we consider the points numbered 5, 6, 7, 8 instead of those numbered 1, 2, 3, 4 since ∇^2 is a symmetric operator. Thus another approximation is

$$\nabla^2 h = \frac{h_5 + h_6 + h_7 + h_8 - 4h_0}{2a^2} \qquad \ldots\ldots\ldots(6)$$

The factor 2 occurs in the denominator because we are now considering a mesh of side $\sqrt{2}\,a$ making an angle $\pi/4$ with the previous mesh. We have denoted quantities such as ζ calculated in these two ways by ζ^+ and $\zeta^\times$, ζ^+ being calculated from the cross formed by the points 0, 1, 2, 3, 4 and $\zeta^\times$ from the St. Andrew's cross formed by the points 0, 5, 6, 7, 8. ζ^+ is the finite difference approximation which is usually used.

The definition of the operator J is

$$J(h,\psi) = \frac{\partial h}{\partial x}\frac{\partial \psi}{\partial y} - \frac{\partial h}{\partial y}\frac{\partial \psi}{\partial x} \qquad \ldots\ldots\ldots(7)$$

/and

and the approximation to J is

$$J(h,\psi) = \frac{(h_1-h_3)(\psi_2-\psi_4)-(h_2-h_4)(\psi_1-\psi_3)}{4a^2} \quad \ldots\ldots\ldots(8)$$

the numbering being as in Fig.1, so that J is a function of the values of h and ψ at the corners of a square. We may compute J from the values at the corners of any other square; thus an alternative approximation is

$$J(h,\psi) = \frac{(h_5-h_7)(\psi_6-\psi_8)-(h_6-h_8)(\psi_5-\psi_7)}{8a^2} \quad \ldots\ldots\ldots(9)$$

and again we distinguish between these two finite difference approximations by writing the first as J^+, the second as $J^\times$. When ψ is $\zeta + f$ we already have two alternative finite difference approximations to it, $\zeta^+ + f$ and $\zeta^\times + f$, and there are four possible Jacobians

$$J^+(h,\zeta^++f),\quad J^+(h,\zeta^\times+f),\quad J^\times(h,\zeta^++f),\quad J^\times(h,\zeta^\times+f)$$

and we denote these by J^{++}, $J^{+\times}$, $J^{\times+}$, $J^{\times\times}$ respectively.
The usual methods of integration of the dynamical equations use J^{++}.

3. The calculations

The values of the vorticities and the Jacobians were calculated from the heights of the 500 mb surface over the mesh of 18 x 14 points in current use in the Forecast Research Division (shown in Fig.4). This is a square grid on a polar stereographic projection with a grid length of approximately 160 miles in the latitude of the British Isles. This gives vorticities over a mesh of 16 x 12 points and Jacobians over a mesh of 14 x 10 points for ζ^+ and J^+, and with points missing in the other fields at the corners of the mesh owing to the methods of calculation. The values which have been computed and which are presented in Tables III and IV are

$$\zeta = \frac{\beta^2 g}{f}\nabla^2 h \quad \ldots\ldots\ldots(10)$$

and are expressed in 10^2 hr^{-1}, β being the map magnification factor on this projection, so that a vorticity given as 064 is 0.64 hr^{-1}. The computed values of the Jacobians are

$$J_{comp} = a^2 J\left(h, \frac{\beta^2 g}{f}\nabla^2 h + f\right) \quad \ldots\ldots\ldots(11)$$

the results being expressed in ft hr^{-1} in Table VII etc. These are the expressions used in the time integrations.

The calculations of vorticities and Jacobians were carried out for 18 cases which had been used to test the Sawyer-Bushby forecasting equations (Sawyer, J.S. and Bushby, F.H. 1953); these cases were used because the data required were readily available in a punched form for use in the electronic computer. It is impracticable to reproduce all the results and in the tables we have given the results for a simple case which appeared to show wider divergences than the average, and which has been used as a test case in several modifications of the Sawyer-Bushby model.

4. Results of the vorticity calculations

It is the absolute vorticity $\zeta + f$, which enters into the forecasting equations, where f is the Coriolis parameter. In some integration schemes the equations are linearised by setting $f+\zeta = f$ where the former occurs as a multiplying factor, so that for some purposes it is better to compare $\zeta^+ - \zeta^x$ with f in order to estimate the importance of the difference. For comparison f is given in Table I in the same units as ζ. On the other hand, in anticyclonic regions where ζ is negative it is better to retain $f + \zeta$ as the comparison with $\zeta^+ - \zeta^x$.

The result which is most apparent is that the field of ζ^x is generally smoother than that of ζ^+ in regions where ζ is large i.e., $|\zeta|$ is of the order of 0.4 hr^{-1}. The patterns are often similar, in that maxima of ζ^+ occur in the same regions as maxima of ζ^x, often at the same grid point, but the maxima of ζ^x are usually less than those of ζ^+. The minima, often small negative values of the order 0.05 hr^{-1}, are more difficult to correlate and are probably of less importance. Occasionally ζ^+, or both ζ^+ and ζ^x were negative and large so that $f + \zeta$ at a grid point was less than zero, and some suspicion must be attached to the analysis near such points, the absolute vorticity being negative; in the time integration negative values of $\zeta + f$ are made zero.

If the height h at a grid point was changed by an amount ϵ, then the resulting change ϵ' in the field of $\zeta^x - \zeta^+$ would have the pattern shown in Fig. 2. A difference of ϵ = 200 ft leads to a value of ϵ' of 0.40 hr^{-1}. In several cases a pattern very similar to that of Fig. 2 was clearly discernible suggesting that perhaps an error had been made in reading off the value of h from the synoptic chart and in one case where both $\zeta^+ + f$, and $\zeta^x + f$ were negative it was found that an error of 200 ft had in fact been made in the height. This property of the field of $\zeta^+ - \zeta^x$ is now used to test the initial data for use in a time integration to detect errors in interpolation. $\zeta^+ - \zeta^x$ is formed and tested to see if it exceeds 0.30 hr^{-1}.

The computations based upon the data at 1500Z 30.1.52 serve as an example of large vorticities and differences which are typical of the results found. The 500 mb height field is given in Table II, and the corresponding contour chart in Fig. 5a while ζ^+, ζ^x and their differences are given in Tables III, IV and V. The region in which both $\zeta^+ + f$ and $\zeta^x + f$ are negative is not typical but these negative values have been closely examined and there would be no justification for redrawing the contour charts to produce positive values of $f + \zeta$, although this could easily be done. The smoothness of the ζ^x field compared with the ζ^+ field in the region of the jet stream shown in Fig. 5a is typical, as are the rather small differences in regions of weak vorticity.

There is a field h' with the same boundary values as h and such that ζ^+ as calculated from h' is the same as ζ^x calculated from h. We calculated the values of ζ^x, integrated the Poisson equation to give the field h' and formed the difference $h-h'$. Table VI gives the difference $h-h'$ for the data of Table II. Originally we intended to carry out the integration for all 18 cases but the first 10 integrations referred to those cases in which the differences $\zeta^x - \zeta^+$ were most marked, so that $h-h'$ would be expected to be greatest. We found in these 10 cases that the maximum value of $h-h'$ was 70 ft over the ocean and this difference was suspect since a change of 200 ft in the height of the 500 mb surface at one grid point over the ocean would have almost cancelled the difference. A closer examination showed that an error of 200 ft had been made in reading the contour height at this point. Apart from this extreme value, the maximum value of $h-h'$ was 50 ft and this was an isolated case (occurring in Table VI). At the 1880 grid points considered the difference $h-h'$ exceeded 20 ft on only 123 occasions and exceeded 40 ft on only 10 occasions, three of which were suspect. We therefore assumed that the differences arising between ζ^+ and ζ^x were no more than could arise from differences between two analyses of the 500 mb chart.

/5.

5. The results of the Jacobian calculations

The calculation of $J(\underline{h}, \zeta)$ involves the height $\underline{h}$ at a number of grid points and the patterns of points used are shown in Fig. 3; we cannot indicate the weight attached to any given point because the Jacobian is a function of two fields. Of these J^{++} uses points which are nearest the origin while J^{XX} uses the most widespread. J^{+X} and J^{XX} have no points in common so that a combination of them will use a compact system with more points than J^{++}, which is also compact.

The Jacobian is formed from first and third derivatives of the height field and is naturally rather rough; however, well marked features in one Jacobian field were generally discernible in the other three fields, although the features were often displaced and of different emphasis. These marked features correspond to some marked feature in the height field such as the presence of a strong jet stream or strongly curved motion.

The maximum absolute value of the Jacobian was 181 ft hr^{-1} and values of 70 ft hr^{-1} were quite common. The differences between the computed values at a given point were often as great as the values themselves, but these large differences were often associated with large differences of the opposite sign in the immediate neighbourhood, there being often a relative displacement of the maxima and minima of the two Jacobian fields. Owing to this relative displacement it is difficult to associate even the sign of the Jacobian with some particular feature in the height field e.g., it is not possible to say that the Jacobian has a particular sign in the rear of a depression, although on general grounds we should expect it to be negative in this region. In straight flow the Jacobian is usually rather small and of indeterminate sign suggesting that there is little change in these regions; the differences were also rather small and of indeterminate sign. There were occasional large Jacobians in flow of a rather indefinite character and these may have been occasioned by small inaccuracies in reading the 500 mb heights at some grid point.

Table VII gives the values of J^{++} calculated for 1500Z 30.1.52 and Tables VIII to X give the differences between the other Jacobians and J^{++}. The eastern and southern parts of the chart have fairly small values of the Jacobians and their difference, and in this region the vorticities and their differences were also small. In the north-west where there is a strong jet stream the differences in the Jacobians are quite marked e.g., at the grid point 5 columns and 5 rows from the north-west corner the following values occur.

J^{++}	$J^{X+} - J^{++}$	$J^{+X} - J^{++}$	$J^{XX} - J^{++}$
181	- 246	-70	- 215

Since the Jacobian has a high negative correlation with the height tendency it is clear that in this region there is a possibility of the different Jacobians leading to different signs of the calculated tendency. The values given in Tables VII to X are fairly representative of the other calculations made.

The J^{XX} field is usually the smoothest, and J^{++} the roughest field; changing the method of calculating the Jacobian makes a greater difference than changing the method of calculating the Laplacian so that the fields J^{++}, J^{+X} were akin as were those of J^{X+} and J^{XX}. The mean of J^{XX} and J^{+X} was found and proved on a whole to be smoother fields than that of any of the other Jacobians. Examination showed that the mean Jacobian fields could be associated with large scale features on the synoptic chart and it may be better to use some mean Jacobian in the time integration.

When considering the vorticity fields we were able to reconstruct the height field corresponding to a given vorticity field and given boundary values; we are unable similarly to reconstruct the height field from the Jacobian field because the differential equation to be solved is not elliptic.

/6.

6. The time integrations

It has been shown above that changing the finite difference scheme can make large differences to the calculated Jacobians. These differences may lead to forecast heights which are quite different; in the example which we have chosen to illustrate the differences it is evident that in some regions the sign of the height tendency will depend upon the finite difference Jacobian used. In order to obtain the height tendency from the Jacobian field a double integration has to be performed and it is possible that this will have a smoothing effect which will remove the differences and lead to much the same values of $\partial h/\partial t$ whatever approximation is used; this is improbable owing to the large differences observed between the Jacobians. It was decided to investigate the effect of using the different vorticities and Jacobians in a 24-hour time integration. The barotropic model affords the simplest computation which involves the vorticities and Jacobians and which leads to results which agree in a fair measure with the development which takes place in the atmosphere. There would be no difficulty in carrying out a baroclinic forecast but it was felt that the extra complication would not help in deciding the effect of using the various finite difference approximations. A programme was therefore written for the solution of

$$\nabla^2 \frac{\partial h}{\partial t} = -J\left(h, \frac{g\nabla^2 h}{f} + f\right) \qquad \ldots\ldots\ldots(12)$$

in which one of four finite difference analogues of the Jacobian can be inserted (at will) on the right hand side. The height h was taken to be the height of the 500 mb surface, f being the Coriolis parameter. The forecasts were made on the usual grid used at Dunstable (shown in Fig.4), the time steps being of one hour; at the boundary we assumed a knowledge of h at $t = 0$, 12 hr and 24 hr and $\partial h/\partial t$ was taken as a constant in each 12-hour period. Values of the Jacobians, tendencies and height fields could be printed out at intermediate times. We chose as the first case for study that which gave the largest differences in the Jacobian fields, the data being those for 1500Z 30.1.52 as in Table I. Two integrations were first carried out using J^{++} and J^{X+} which showed the greatest differences at time $t = 0$; the differences in the 24-hour forecast were sufficiently large to make it worthwhile to carry out the integrations using J^{+X} and J^{XX} also.

Table IX gives the predicted height of the 500 mb surface at the inner 140 points using the four methods of calculating the Jacobian and two of the corresponding contour charts are shown in Fig. 5. The forecast made using J^{++} and that made using J^{+X} are almost identical; the greatest difference is 150 ft with 7 differences of over 100 ft and 103 of 50 ft or less. Similarly the forecasts using J^{X} are almost identical, with a greatest difference of 150 ft, 6 differences of 100 ft or more and 111 of 50 ft or less. On the other hand the greatest difference between the forecast made using J^{++} and that made using J^{X+} is 720 ft, with 49 differences of 100 ft or more and only 51 of 50 ft or less. Table X gives the root mean square differences between the different forecasts. The large differences in the forecasts arise between those using a J^{+} and those using a J^{X} and we need consider only the differences between J^{++} and J^{X+}, the differences between J^{+X} and J^{XX} being similar, while those between J^{++} and J^{+X} are small.

The height field was printed out at each 3-hour interval, the vorticity, Jacobian and the tendency fields being printed at each 6-hour interval. The maximum differences between J^{++} and J^{X+}, which were initially large, decreased, the largest difference falling from -246 at $t = 0$ to 155 at $t = 12$ hr and -157 at $t = 24$ hr. The root mean square differences over the 140 points considered decreased at first but increased again, showing that the differences were increasing over most of the chart. The R.M.S. differences between J^{++} and J^{X+} were 45 ft hr^{-1} at $t = 0$, 33 ft hr^{-1} at $t = 12$ hr and 46 ft hr^{-1} at $t = 24$ hr.

/The

The computed initial fields of $\partial h/\partial t$ using J^{++} and J^{X+} are given in Table XI. The double integration has considerably smoothed out the roughness of the original Jacobian fields and the bottom four rows of each table are very much the same. The calculated rises in the rear of the depression are larger when J^{++} is used than when J^{X+} is used by the order of 10 ft hr^{-1} and the maximum rise is displaced further south by a grid length. The falls ahead of the low towards Scotland are also larger by about the same amount so that even at this stage it will not be surprising if the final forecasts differ considerably. The 6-hour forecasts of the height of the 500 mb surface are very similar, since the differences in $\partial h/\partial t$ can lead only to differences in height of 50-100 ft ahead of and behind the low; there is a slight but noticeable difference in the trough position.

The fields of $\partial h/\partial t$ after 6 hr are given in Table XII and at this stage the difference in the isopleths in the upper central part of the field is quite marked, with the forecast using J^{++} moving the trough more rapidly eastwards with a greater surge of pressure behind.

The 12-hour forecasts are given in Table XIII and show the trough further east and north when J^{++} is used, the jet being almost west to east. The forecast made with J^{X+} holds the trough further back, extending it southward. At this stage we are effectively starting a 12-hour forecast with different initial charts using different methods of calculation and the divergence continues to grow.

The computed values of the tendency field after 24 hr are given in Table XIV; that computed using J^{++} is out of phase with that computed using J^{X+}, the centres having been moved further east and now appearing less intense. The differences between the fields have increased, the R.M.S. values being 11, 17 and 22 ft hr^{-1} at times $\underline{t}$ = 0, 12, 24 hr respectively, and the difference field is as great as the fields themselves. It is clear that further time integration would lead to more widely divergent forecasts.

The height field of the 500 mb surface at 1500Z 30.1.52 has been given in Table II, as has the height field 24 hr later. The forecast height fields have been given in Table IX; the fields are shown in chart form in Fig. 5(a), (b), (c), (d). The differences between the forecast and actual height values show that the forecast made using J^{X+} was superior to that made using J^{++}, the maximum errors being 970 ft and 1290 ft respectively. The differences between the forecast values are not quite as great as the difference between the better forecast values and the actual final values, but are of the same order in the vicinity of the trough; near the boundaries in the north-west both forecast values are similar and differ from the actual values by several hundred feet.

In the region of the trough the differences between the forecast values are large; the maximum difference is 730 ft and at eight grid points the difference exceeds 400 ft. These large differences occur because the forecast made using J^{++} moved the trough too far east without sufficient deepening and failed to predict the south-eastward extension. The forecast made using J^{X+} predicted part of the south-eastward extension and moved the trough more slowly in accordance with the actual development, the failure being mainly in the failure to forecast the considerable deepening in the region of the British Isles. The increasing difference between the two forecasts is borne out by the R.M.S. differences between them, which are 103 ft after 12 hr and 177 ft after 24 hr.

In order to compare the two forecasts with one another and also with forecasts made from the same initial data using other methods of computation, the actual and forecast height changes have been correlated over the inner grid of 12 x 8 points, and the resulting correlation coefficients are given in Table XV. There is marked difference in the correlation coefficients indicating that the forecast made using J^{X+} was superior to that made using J^{++} and this is borne out synoptically by the charts shown in Fig. 5. The improvement made by using J^{X+} instead of J^{++} is as marked as is that made by any of the changes made in the method of use of the Sawyer-Bushby model.

/7.

7. Some further results

The synoptic situation of 30.1.52 is characterized by a strong jet stream; the existence of a jet is common although perhaps that occurring in this situation is stronger than usual. Similar experiments with two quite different synoptic situations and developments were carried out.

The initial chart used in the first of these refers to 1500Z 27.1.52 and is given with the chart 24 hr later at 1500Z 28.1.52 in Fig.6(a) and (b). Initially there was a low to the west of Iceland with its attendant trough stretching SSE. The ridge ahead of it was to the west of Ireland with a deep trough extending down the North Sea, through the Low Countries and curving backward into Spain. In the next 24 hr the trough extending from the Iceland low developed and lay down the Irish Sea, while the deep trough over the North Sea moved eastward and relaxed. The ridge between these two troughs moved off the eastern coasts of Great Britain and also relaxed so that the amplitude of the pattern was reduced. The 24-hour changes in the height of the 500 mb surface were generally less than those which occurred in the 24 hr following 1500Z 31.1.52.

The 24-hour forecasts made with the use of J^{++} and J^{X+} are given in Fig.6 (c) and (d). The 24-hour changes in height of the 500 mb surface over and to the west of Great Britain were not more than about 300 ft so that minor differences in the forecast changes could lead to large differences in the positions of the relaxing trough and ridge; the pattern of height changes, a slight fall to the west of Great Britain and a rise to the east was well forecast by both the numerical methods. Table XVI, which gives a statistical summary of the three time integrations, shows the high correlation between observed and forecast changes. The difference between the forecast height changes increased with time and was in the mean about 40 per cent of the actual change. Thus, although there appears to be little difference in the success of the two methods of forecasting as judged by the correlation coefficients, the forecast height changes at many points on the chart are different in magnitude and the troughs and ridge are relatively displaced.

The last synoptic situation chosen for examination refers to 1500Z 30.1.53. On the night of 31.1.53 strong NW. winds in the North Sea caused disastrous flooding on the east coast of Great Britain and on the coasts of Holland and Denmark. Numerical forecasts had already been made using the data of 1500Z 30.1.53 and we chose to make two barotropic forecasts from the same data. At this time a deep trough with strong NW. winds stretched almost due south from Iceland with a ridge ahead over the North Sea, Great Britain being in a SW. airstream of about 50 knots. In 24 hr the trough developed rapidly, and advanced with a closed centre over the southern North Sea and very strong N. and NW. winds over Great Britain, reaching 119 knots at Larkhill, while a strong ridge almost replaced the trough.

The synoptic situations at 1500Z 30.1.53 and 1500Z 31.1.53 are shown in Fig.7(a) and (b), the numerical forecasts using J^{++} and J^{X+} being given in Fig.7(c) and (d). The pattern of changes, a rapid fall in the region of Great Britain and the North Sea with a rapid rise to the west, was well forecast, giving a high correlation coefficient between the forecast and actual changes in each case. As in Table XVI however, the resulting forecast charts showed the trough too far west and under-emphasized both the depth and the very strong northerly winds which were the most important feature of the synoptic situation. The R.M.S. of the difference between the forecast height changes again increased almost linearly with time, but were only about 10 per cent of the actual changes after 24 hr. The forecast made using J^{++} was, from a synoptic point of view, more successful than that made using J^{X+} since it moved the trough further east and gave a lower pressure within it; neither forecast gave the closed low that actually existed after 24 hr.

/8.

8. Conclusion

In the experiment which has been described above two sets of forecasts have been made from the same data using the same method, the only difference introduced being in the orientation and length of the mesh. The 24-hour forecast on two of the three occasions differed considerably in an area near the centre of the mesh which is usually supposed to be the most free from errors which arise because of the boundary conditions. The difference between the two forecast values of the changes in the height field of the 500 mb surface increased with time and was about 40 per cent of the actual change in two cases and about 10 per cent in the third. The implication is grave, that upon some occasions the choice of mesh size and orientation in the field has a decisive effect upon the forecast that is made. There can be little doubt that the differences depend very largely upon the computed Jacobians and the remedy may lie in a more accurate determination of derivatives by taking into account values at more grid points in computing them. Further experiments will be carried out to point to a solution of the difficulty.

LIST OF TABLES

TABLE I — Values of the Coriolis parameter, f, at the grid points of Fig.4 ($10^{-2}hr^{-1}$).

II(a) — Contour heights of 500 mb surface at 1500Z 30.1.52 at grid points of Fig.4 (tens of feet, the initial unit figure omitted).

II(b) — Contour heights of 500 mb surface at 1500Z 31.1.52 corresponding to those in the inner rectangle above.

III — Relative vorticity ζ^{+} 1500Z 30.1.52 ($10^{-2}hr^{-1}$) for the grid of Fig.3 calculated from points 0, 1, 2, 3, 4 of Fig.1.

IV — Relative vorticity ζ^{x} 1500Z 30.1.52 ($10^{-2}hr^{-1}$) for the same grid as Table III calculated from points 0, 5, 6, 7, 8 of Fig.1.

V — Relative vorticity differences $\zeta^{x} - \zeta^{+}$ 30.1.52 ($10^{-2}hr^{-1}$).

VI — Height differences in feet calculated from relaxation of Table V, 1500Z 30.1.52.

VII — Computed Jacobian J^{++} (ft hr^{-1}) 1500Z 30.1.52.

VIII(a) — The difference $J^{x+} - J^{++}$ (ft hr^{-1}) 1500Z 30.1.52.

VIII(b) — The difference $J^{+x} - J^{++}$ (ft hr^{-1}) 1500Z 30.1.52.

VIII(c) — The difference $J^{xx} - J^{++}$ (ft hr^{-1}) 1500Z 30.1.52.

IX(a) — Predicted heights of 500 mb surface at 1500Z 31.1.52 at the 14 x 10 inner grid points using J^{++} (tens of feet, the initial unit figure being omitted).

IX(b) — Predicted heights of 500 mb surface at 1500Z 31.1.52 at the 14 x 10 inner grid points using J^{x+} (tens of feet, the initial unit figure being omitted).

IX(c) — Predicted heights of 500 mb surface at 1500Z 31.1.52 at the 14 x 10 inner grid points using J^{+x} (tens of feet, the initial unit figure being omitted).

IX(d) — Predicted heights of the 500 mb surface at 1500Z 31.1.52 at the 14 x 10 inner grid points using J^{xx} (tens of feet, the initial unit figure being omitted).

X — The R.M.S. difference between 24-hour forecasts using different Jacobians.

XI(a) — Values of $\partial h/\partial t$ computed using J^{++} 1500Z 30.1.52 (ft hr^{-1}).

XI(b) — Values of $\partial h/\partial t$ computed using J^{x+} 1500Z 30.1.52 (ft hr^{-1}).

XII(a) — Values of $\partial h/\partial t$ computed using J^{++} 2100Z 30.1.52 (ft hr^{-1}).

XII(b) — Values of $\partial h/\partial t$ computed using J^{x+} 2100Z 31.1.52 (ft hr^{-1}).

XIII(a) — Predicted heights of 500 mb surface at 0300Z 31.1.52 using J^{++} (tens of feet).

XIII(b) — Predicted heights of 500 mb surface at 0300Z 31.1.52 using J^{x+} (tens of feet).

XIV(a) — Values of $\partial h/\partial t$ computed at 1500Z 31.1.52 using J^{++} (ft hr^{-1}).

XIV(b) — Values of $\partial h/\partial t$ computed at 1500Z 31.1.52 using J^{x+} (ft hr^{-1}).

XV — Correlation of forecast height change with actual height change.

XVI — Statistical summary.

TABLE I

Values of the Coriolis parameter, f, at the grid points of Fig. 4 ($10^{-2}hr^{-1}$)

045	045	046	047	047	048	048	048	048	048	048	048	047	047	046	045
044	044	045	046	046	047	047	047	047	047	047	047	046	046	045	044
043	043	044	045	045	046	046	046	046	046	046	046	045	045	044	043
041	042	043	044	044	044	045	045	045	045	045	044	044	044	043	042
040	041	042	042	043	043	044	044	044	044	044	043	043	042	042	041
039	040	040	041	041	042	042	042	043	042	042	042	041	041	040	040
038	038	039	040	040	040	041	041	041	041	041	040	040	040	039	038
036	037	038	038	039	039	039	039	039	039	039	039	039	038	038	037
035	036	036	037	037	037	038	038	038	038	038	037	037	037	036	036
033	034	035	035	035	036	036	036	036	036	036	036	036	035	035	034
032	033	033	034	034	034	035	035	035	035	035	034	034	034	033	033
030	031	032	032	032	033	033	033	033	033	033	033	032	032	032	031

TABLE II (a)

Contour heights of 500 mb surface at 1500Z 30.1.52 at grid points of Fig.4 (tens of feet, the initial unit figure omitted)

662	648	624	613	609	619	641	670	691	704	704	704	704	697	697	706	716	730
682	668	629	602	575	587	603	642	686	704	706	706	704	699	699	709	721	735
706	692	640	600	570	570	587	615	670	705	719	715	708	705	709	716	728	743
735	718	684	632	594	584	592	618	669	711	730	728	717	716	722	726	733	751
774	765	735	695	654	630	630	648	687	718	737	743	732	730	730	734	740	760
817	816	798	760	722	691	678	686	706	727	743	753	748	743	739	746	758	772
850	849	843	826	803	778	749	738	743	757	766	766	762	757	758	766	774	784
885	878	870	859	846	831	815	803	795	790	785	777	770	770	775	781	786	794
912	908	897	887	876	864	851	839	822	810	802	788	779	781	787	791	797	803
926	922	915	905	894	883	871	859	840	824	812	801	792	791	795	799	804	810
937	931	927	919	909	897	885	870	852	835	819	810	804	801	803	806	811	814
943	939	932	925	916	905	892	876	859	840	825	815	809	807	810	813	818	822
946	942	936	928	920	909	891	876	862	845	827	817	812	813	816	819	824	829
948	943	937	928	921	909	891	875	862	848	832	818	817	818	821	825	830	836

TABLE II (b)

Contour heights of 500 mb surface at 1500Z 31.1.52 corresponding to those in the inner rectangle above

654	622	610	615	621	633	636	649	666	682	682	682	695	711
674	640	621	615	613	614	618	634	653	672	687	693	699	713
708	675	654	644	639	636	637	643	650	664	681	695	708	721
749	730	713	702	694	682	670	661	655	658	677	695	711	728
815	810	792	773	752	732	716	699	679	669	679	698	719	736
866	865	855	837	821	791	760	742	725	698	696	713	733	750
902	901	893	876	856	835	812	785	759	743	734	740	753	764
914	911	909	905	889	870	846	825	801	776	771	773	772	777
921	921	917	911	906	898	878	853	834	816	805	796	789	788
923	922	921	918	913	906	897	880	855	838	821	811	802	800

TABLE III

Relative vorticity ζ^+ 1500Z 30.1.1952 ($10^{-2}hr^{-1}$) at the grid points of Fig.3 calculated from grid points 0, 1, 2, 3, 4, of Fig.1

-021	017	008	062	017	039	005	-032	-013	008	004	001	008	016	006	004
-037	045	043	056	044	029	051	-004	-014	-018	001	008	011	006	008	001
004	-012	046	064	049	049	049	009	-021	-023	-007	015	010	-007	001	014
-019	002	001	026	040	028	029	-007	-010	-014	-022	010	001	005	006	028
-042	-044	001	022	047	047	027	020	017	011	-013	-002	002	023	015	000
-012	-036	-047	-047	-044	015	032	027	-002	-014	-007	-008	006	006	-006	-002
000	-004	-009	-019	-026	-031	-030	-026	-015	-006	001	010	004	-005	-008	003
-034	-011	-015	-017	-020	-019	-027	-005	-003	-016	009	019	004	-008	000	-006
-013	-014	-007	-004	-008	-008	-022	-004	001	-003	-003	010	007	000	000	002
002	-018	-016	-016	-009	-015	-012	-006	-007	009	-001	-006	002	000	003	-003
-015	-002	-009	-008	-010	-018	-011	-010	006	002	002	003	008	-002	002	-004
-008	-010	-006	-011	-020	007	-004	-010	-005	019	007	014	002	-002	004	000

Note that vorticities are given on a grid of 16 x 12 points formed from the grid of Fig.3 by omitting the outer ring of points.

TABLE IV

Relative vorticity $\zeta^{\times}$ 1500Z 30.1.1952 ($10^{-2}hr^{-1}$) for the same grid points as Table III calculated from grid points 0, 5, 6, 7, 8 of Fig.1

018	016	046	026	027	009	-021	-014	002	005	002	010	013	007	005
-020	030	040	059	039	038	040	-002	-013	-012	-001	008	010	007	005	005
-009	008	036	059	051	045	048	005	-014	-018	-008	012	007	-001	002	011
-015	-008	010	027	034	030	026	-003	-012	-014	-017	006	003	006	009	019
-038	-033	-003	023	039	043	034	019	013	006	-008	002	005	017	010	007
-017	-037	-041	-042	-029	008	023	019	001	-009	-010	-003	002	005	-004	-002
-007	-007	-011	-018	-027	-025	-028	-021	-016	-011	001	007	004	-003	-005	000
-026	-017	-016	-017	-020	-018	-022	-008	-005	-010	004	015	005	-005	-003	-003
-012	-011	-008	-006	-008	-010	-018	-004	-001	-003	000	008	006	-001	001	-002
-007	-014	-015	-014	-011	-013	-013	-007	-003	003	-001	-001	002	-002	002	000
-009	-007	-007	-009	-012	-013	-011	-008	000	006	002	004	006	-001	002	-004
-008	-009	-006	-012	-014	-001	000	-010	-002	011	013	009	005	-001	003	

TABLE V

Relative vorticity differences $\zeta^{\times} - \zeta^{+}$ 30.1.1952 ($10^{-2}hr^{-1}$)

000	008	-015	009	-012	004	010	-001	-006	000	001	002	-004	001	001
018	-015	-003	003	-006	009	-011	002	001	006	-002	-000	-001	001	-002	004
-014	020	-010	-004	002	-003	-001	-005	006	005	-001	-003	-002	005	001	-003
005	-010	009	001	-006	002	-002	004	-002	-000	005	-004	002	001	002	-008
005	011	-004	001	-009	-003	007	-001	-004	-005	005	004	003	-006	-005	007
-005	-001	006	005	014	-006	-009	-008	003	005	-003	005	-003	-001	002	001
-007	-003	-002	001	-002	007	002	005	-001	-005	-001	-002	000	002	003	-003
007	-006	-001	000	000	001	004	-003	-003	006	-004	-005	001	003	-003	003
001	002	-001	-002	001	-001	004	000	-002	001	003	-001	-001	-001	001	-003
-009	004	001	002	-002	002	-001	-001	-004	006	000	004	000	-002	-001	003
006	-005	002	-001	-002	005	000	002	-006	004	000	001	-002	001	000	000
000	001	000	-001	005	-008	004	001	003	-008	006	-005	003	001	-001	

TABLE VI

Height differences in feet calculated from relaxation of Table V 1500Z 30.1.1952

004	-001	050	003	037	-002	-036	-011	007	-002	-004	-003	008	-001	-006
-034	030	029	027	031	009	034	-011	-024	-030	-004	002	003	-002	003	-007
012	-030	029	035	026	028	024	007	-030	-034	-010	008	004	-014	-001	009
-012	001	-012	013	036	022	018	-002	-002	-012	-022	000	-007	-002	002	019
-020	-033	-010	-002	026	023	004	012	014	007	-019	-020	-009	015	011	-008
006	-010	-027	-031	-033	013	029	028	005	-004	002	-012	004	005	-004	-004
014	007	-004	-016	-017	-021	-007	-002	008	015	012	010	002	-006	-007	001
-007	010	001	-006	-012	-018	-018	001	008	-001	016	017	002	-007	000	-004
-001	-002	000	000	-007	-010	-017	-002	007	006	003	007	003	000	-002	002
011	-004	-004	-004	-002	-011	-006	-002	-001	012	002	-006	001	003	000	-005
-004	005	-002	-001	-001	-010	-006	-003	009	001	-001	-001	003	-001	000	-001
-001	-001	-001	-001	-006	006	-006	-003	-001	010	-005	005	-002	-002	-000	

TABLE VII

Computed Jacobian J^{++} (ft hr^{-1}) 1500Z 30.1.52

041	071	001	-011	-010	-067	-060	010	018	011	006	-001	004	001
005	083	-031	-021	004	016	-018	-014	006	019	009	-013	-004	009
001	-015	056	006	-021	-024	-049	-046	-024	014	011	-004	-001	008
064	126	046	000	-060	-060	-046	-013	-019	-009	006	017	008	-013
-039	-037	-039	116	181	027	-053	-044	-001	005	009	009	-004	002
000	-003	-010	-009	-034	-016	018	026	013	013	005	-009	-004	003
016	-006	003	008	003	024	041	-003	008	018	-004	-015	-003	-001
001	006	-001	002	-010	013	014	-005	011	000	-001	-005	-004	000
-004	000	000	-002	-010	010	-006	008	003	-005	-001	002	001	-001
004	002	001	-011	014	006	-003	002	003	003	004	-002	-002	-001

Note that Jacobians are given on a grid of 14 x 10 points formed from the grid of Fig. 3 by omitting the two outer rings of points, and correspond to the points inside the rectangle shown in Table II(a).

TABLE VIII (a)

The difference $J^{x+} - J^{++}$ (ft hr^{-1}) 1500Z 30.1.52

051	-043	027	008	-028	040	038	-013	-009	-006	-003	-001	-006	004
076	-114	042	001	006	-034	011	011	000	-006	-004	011	006	-010
038	151	-018	-004	006	-028	-001	009	013	-006	-004	005	002	-011
-106	-189	-066	064	147	031	-016	-026	009	019	007	-015	-010	023
089	099	033	-151	-246	-050	074	066	-004	-005	-003	-006	006	-003
-009	010	033	071	099	031	-031	-063	-009	004	-003	004	-001	-002
-020	004	-008	-007	-008	-005	-014	018	-002	-010	006	008	-003	003
006	-009	003	-002	013	-004	-003	012	-012	004	-001	000	004	-001
006	002	-003	-008	008	-015	018	-008	-003	006	004	-005	-003	002
-006	000	-003	020	-016	-002	004	003	000	000	-004	000	003	001

TABLE VIII (b)

The difference $J^{+x} - J^{++}$ (ft hr^{-1}) 1500Z 30.1.52

017	-018	007	003	-009	014	029	-008	-005	-004	-001	001	-003	001
021	-032	022	002	003	-017	-001	008	-001	-004	-002	006	001	-004
-004	045	-039	-004	-008	-007	-007	011	009	-002	000	003	001	-003
-011	-039	-009	009	045	010	-003	-009	003	006	001	-008	-005	011
013	017	026	-031	-070	-005	023	018	-006	-001	-002	-005	003	-001
004	001	-004	002	014	002	-003	-014	001	001	-001	002	001	-001
-006	007	-001	003	001	-003	-011	007	001	-005	004	004	-001	000
003	-003	002	-001	003	-003	-003	005	-005	002	000	001	002	-001
002	000	-001	-002	005	-004	004	-006	002	003	001	-003	000	002
-003	001	-003	007	-008	004	000	000	001	002	-003	000	001	000

TABLE VIII (c)

The difference $J^{xx} - J^{++}$ (ft hr^{-1}) 1500Z 30.1.52

	-034	019	005	-020	043	036	-011	-011	-005	-004	000	-006	003
056	-079	031	006	003	-031	009	014	000	-009	-003	012	005	-009
053	094	-011	-006	019	-030	-001	014	015	-006	-003	004	000	-009
-093	-152	-064	046	119	038	-005	-018	010	019	004	-016	-008	019
081	082	031	-143	-215	-049	060	053	000	-001	-004	-008	004	001
-006	016	032	061	078	028	-026	-047	-014	-001	-001	005	000	-003
-016	004	-006	-006	-002	-009	-019	013	001	-008	006	009	-001	001
004	-006	002	000	013	-006	-003	009	-011	003	001	001	003	000
006	000	-003	-003	007	-013	012	-005	-003	006	003	-005	-002	001
-004	-002	-001	015	-011	-005	007	001	002	-001	-004	000	002	-

TABLE IX (a)

Predicted heights of 500 mb surface at 1500Z 31.1.52 at the 14 x 10 inner grid points using J^{++} (tens of feet, the initial unit figure being omitted)

663	656	640	625	623	620	649	657	664	671	675	681	695	708
680	673	659	647	644	639	640	639	639	656	668	684	702	715
719	710	699	692	682	681	675	672	672	672	671	688	713	726
752	747	747	745	733	731	735	737	731	730	715	716	725	742
810	800	800	798	788	781	785	792	789	791	766	761	751	762
859	850	848	841	830	824	824	824	823	827	806	795	778	776
899	893	887	878	867	861	859	857	858	852	834	818	799	787
913	912	910	901	895	886	884	883	882	869	850	831	808	794
923	926	922	919	913	901	899	895	890	880	861	830	809	800
925	925	926	922	921	918	915	906	896	886	862	835	818	808

TABLE IX (b)

Predicted heights of 500 mb surface at 1500Z 31.1.52 at the 14 x 10 inner grid points using J^{x+} (tens of feet, the initial unit figure being omitted)

671	650	638	622	617	616	636	651	665	672	676	683	697	715
691	674	664	651	632	614	618	625	643	658	675	690	708	719
718	714	701	695	677	658	641	633	638	654	677	700	716	721
761	753	755	739	731	726	708	692	671	671	691	715	728	733
810	810	794	788	782	778	782	767	743	718	719	738	744	750
856	856	849	832	823	832	831	825	807	779	763	761	761	766
889	891	883	868	863	869	872	865	856	830	800	784	775	776
912	909	910	894	886	894	901	894	883	856	832	803	789	785
923	922	914	908	903	907	914	910	893	866	841	818	802	794
924	925	922	922	919	923	925	918	899	872	850	828	811	802

TABLE IX (c)

Predicted heights of 500 mb surface at 1500Z 31.1.52 at the 14 x 10 inner grid points using J^{+x} (tens of feet, the initial unit figure being omitted)

662	644	631	629	629	622	641	655	665	671	677	684	699	710
681	667	667	662	654	640	628	631	638	656	672	689	706	717
718	706	706	701	686	673	663	662	658	663	676	703	718	726
764	754	743	742	737	738	731	728	729	717	708	727	736	741
807	809	802	794	781	785	785	783	794	783	761	761	759	764
855	852	850	837	827	823	821	823	834	827	803	792	779	777
896	892	887	876	867	859	859	861	865	854	833	814	796	787
913	913	908	902	893	885	887	889	886	874	851	826	805	795
924	925	923	918	909	903	902	900	893	879	854	828	810	802
924	926	926	922	921	920	918	908	896	879	855	834	818	808

TABLE IX (d)

Predicted heights of the 500 mb surface at 1500Z 31.1.52 at the 14 x 10 inner grid points using J^{xx} (tens of feet, the initial unit figure being omitted)

669	651	636	620	617	616	639	654	669	676	680	687	700	713
691	677	671	643	627	616	621	631	649	666	682	696	711	719
718	711	708	695	677	660	645	636	643	666	689	708	719	723
761	761	753	737	725	729	712	693	674	682	706	726	730	735
808	805	801	798	785	780	776	765	740	723	733	747	749	753
859	857	840	832	833	832	836	827	809	779	766	767	766	768
890	890	881	867	866	872	875	873	861	828	800	787	779	779
915	911	904	892	891	900	908	905	887	856	826	804	792	788
923	922	915	907	908	913	918	913	893	864	839	816	802	795
924	926	923	922	922	925	926	916	898	871	848	828	812	803

TABLE X

The R.M.S. difference between 24-hour forecasts using different Jacobians

Forecasts using	J^{X+}, J^{++}	J^{+X}, J^{++}	J^{X+}, J^{XX}
R.M.S. difference (ft)	177	54	47

TABLE XI (a)

Values of $\partial h/\partial t$ computed using J^{++} 1500Z 30.1.52 (ft hr^{-1})

029	055	034	011	-011	-043	-050	-029	-015	-008	-007	-006	-003	001
028	064	034	010	-010	-034	-054	-046	-026	-008	-003	-007	-002	006
029	055	060	027	-011	-043	-066	-062	-041	-013	-003	-002	001	006
041	081	069	043	002	-036	-057	-050	-036	-016	-001	005	003	-001
011	031	036	071	073	014	-029	-033	-016	-004	003	003	-002	-003
009	019	025	037	031	019	013	009	008	009	004	-003	-005	-004
011	016	023	030	031	036	036	021	018	016	003	-006	-008	-007
010	016	019	023	024	033	033	024	021	014	004	-004	-008	-008
008	013	015	017	019	027	024	024	020	013	006	-001	-007	-009
008	011	012	011	020	021	019	020	021	016	009	-003	-009	-011

TABLE XI (b)

Values of $\partial h/\partial t$ computed using J^{X+} 1500Z 30.1.52 (ft hr^{-1})

044	045	041	015	-014	-030	-034	-026	-016	-011	-008	-006	-004	001
049	045	041	014	-008	-037	-044	-037	-021	-008	-004	-004	-001	003
041	076	054	027	-005	-047	-062	-053	-031	-009	-001	-001	001	003
014	029	034	041	023	-029	-053	-046	-026	-007	003	001	001	004
028	045	033	022	003	-011	-014	-014	-011	-002	003	001	-001	-002
015	032	038	046	040	020	003	-007	001	008	004	-001	-005	-004
009	021	026	033	031	032	027	018	013	011	004	-003	-007	-006
011	016	021	024	027	030	029	023	016	013	004	-004	-006	-008
010	013	015	016	020	023	027	021	018	013	006	-003	-008	-008
006	011	012	016	016	019	020	021	020	016	008	-003	-009	-010

TABLE XII (a)

Values of $\partial h/\partial t$ computed using J^{++} 2100Z 30.1.52 (ft hr^{-1})

015	028	043	031	005	-017	-030	-032	-024	-015	-009	-008	-004	001
-014	025	069	048	014	-007	-039	-061	-054	-026	-009	-007	-006	003
-018	022	068	040	030	011	-036	-064	-066	-039	-011	-003	000	002
-019	019	043	058	089	056	006	-036	-048	-038	-013	001	006	002
-016	-004	019	046	052	053	063	009	-021	-014	-002	005	001	001
-008	-003	011	021	029	048	044	018	013	015	014	005	-002	-004
-001	006	010	017	028	035	041	039	032	031	020	004	-004	-006
006	011	013	019	024	029	044	041	037	031	016	003	-005	-008
008	011	013	019	018	027	036	035	033	024	011	002	-004	-008
006	009	012	014	019	026	028	029	026	019	009	-001	-008	-010

TABLE XII (b)

Values of $\partial h/\partial t$ computed using J^{x+} 2100Z 31.1.52 (ft hr^{-1})

017	038	048	026	004	-013	-027	-031	-024	-016	-011	-008	-005	001
-001	048	057	031	014	-014	-042	-053	-041	-022	-009	-005	-002	001
-007	019	047	043	028	-004	-051	-069	-054	-027	-008	-002	-001	001
-029	029	066	049	033	008	-027	-047	-044	-023	-005	001	001	001
-016	-018	021	044	043	031	000	-023	-032	-015	-001	002	-001	-003
-010	006	023	031	029	015	009	-001	-003	002	004	001	-004	-003
-004	001	016	027	032	031	028	020	011	013	008	-001	-006	-006
004	007	014	021	028	031	036	032	022	015	008	-001	-006	-008
007	009	011	016	021	026	033	030	024	015	009	-001	-006	-009
006	010	011	016	018	024	026	025	021	015	011	-001	-009	-011

TABLE XIII (a)

Predicted heights of 500 mb surface at 0300Z 31.1.52 using J^{++} (tens of feet)

659	642	616	601	592	593	633	668	690	697	696	696	704	716
682	670	650	631	609	607	624	646	671	698	705	707	716	728
734	714	702	685	661	648	649	655	668	697	716	725	730	736
788	775	771	760	739	724	711	699	698	712	730	743	745	748
830	822	818	818	812	793	783	768	754	752	759	762	759	767
864	857	853	852	847	839	833	819	803	793	785	776	773	777
897	892	886	882	877	872	866	852	836	821	803	786	783	784
921	917	908	902	895	889	886	868	853	836	812	795	790	791
936	931	923	916	904	898	890	873	856	840	819	804	798	797
940	936	930	920	913	904	890	873	856	838	820	807	801	801

TABLE XIII (b)

Predicted heights of 500 mb surface at 0300Z 31.1.52 using J^{X+} (tens of feet)

661	641	624	599	590	598	639	670	691	696	695	696	704	717
690	677	653	620	605	600	622	651	684	701	706	710	720	728
732	725	711	679	656	638	632	644	676	710	721	727	729	735
781	782	774	745	718	695	678	676	692	723	740	742	739	747
834	817	822	816	790	767	745	736	732	747	759	758	756	762
867	866	859	865	853	827	809	791	782	777	773	770	770	777
894	891	890	890	887	877	854	835	817	802	788	780	780	784
921	913	908	904	902	895	881	861	838	819	802	790	789	790
935	930	921	914	908	900	889	870	848	829	815	800	795	796
939	936	928	923	913	904	890	870	851	834	821	806	800	800

TABLE XIV (a)

Values of $\partial h/\partial t$ computed at 1500Z 31.1.52 using J^{++} (ft hr^{-1})

-001	001	016	019	019	026	022	001	-012	-019	-020	-016	-009	-008
-004	-001	012	004	011	025	022	009	-008	-019	-029	-031	-018	-010
-010	-006	-006	002	007	009	019	009	011	019	-009	-040	-035	-011
-024	-039	-043	-003	008	-023	-026	004	014	029	029	-005	-031	-012
-009	-014	-036	-004	016	-012	-043	-021	-003	031	031	011	-011	-006
007	-003	-011	015	016	-007	-018	-014	-023	009	023	020	004	006
004	006	011	022	014	-002	-009	-016	-014	015	021	024	017	013
-006	-003	008	013	010	006	-006	-009	005	021	021	038	032	014
-012	-005	004	007	015	010	001	006	015	024	029	034	019	008
-013	-009	-001	004	011	012	015	023	034	056	060	036	018	010

TABLE XIV (b)

Values of $\partial h/\partial t$ computed at 1500Z 31.1.52 using J^{x+} (ft hr^{-1})

010	009	009	016	022	014	-002	-012	-016	-018	-018	-014	-008	-002
-001	012	011	021	019	009	-002	-011	-020	-031	-031	-024	-017	-008
-014	-012	-003	016	009	005	001	001	-008	-033	-043	-036	-020	-012
-031	-010	000	-006	009	-008	-008	006	015	-011	-046	-042	-018	-014
-029	-032	-001	018	-032	-030	000	018	038	004	-031	-031	-018	-011
-023	-011	016	-003	-028	-048	-025	014	039	041	-002	-014	-011	-009
-009	-009	014	018	-028	-048	-021	004	036	038	026	011	-003	-004
-009	-003	012	009	-015	-029	-014	012	034	048	041	021	006	-001
-011	-006	-001	003	-008	-011	004	022	033	041	033	028	011	002
-013	-009	-003	000	002	006	020	038	051	051	043	030	016	004

TABLE XV

Correlation of forecast height change with actual height change

	Method of forecast	Correlation coefficients
(a)	Barotropic using J^+	+0.48
(b)	" " J^X	+0.72
(c)	Sawyer-Bushby model (500 mb, zero boundary changes	+0.61
(d)	" " " (600 mb, zero boundary changes	+0.59
(e)	" " " (500 mb, zero boundary changes, heating effect	+0.62
(f)	" " " (600 mb, actual boundary changes, heating effect	+0.47
(g)	Stream function (600 mb, actual boundary changes, heating effect	+0.76

TABLE XVI

Statistical summary

		Forecast commencing at 1500Z		
		30.1.52	27.1.52	30.1.53
Correlation of forecast and actual 24-hour height changes at 500 mb	J^{++}	0.48	0.94	0.95
	J^{x+}	0.72	0.91	0.92
Using Sawyer-Bushby model*		0.47	0.93	0.96
R.M.S. of forecast height differences using J^{++} and J^{x+}	12 hr	103 ft	37 ft	59 ft
	24 hr	177 ft	73 ft	96 ft
R.M.S. actual change	24 hr	401 ft	256 ft	624 ft
Ratio $\frac{\text{R.M.S. (difference between 24-hour forecasts)}}{\text{R.M.S. (actual 24-hour change)}}$		0.44	0.39	0.12
$\frac{\sigma \text{ (forecast 24-hour change)}}{\sigma \text{ (actual 24-hour change)}}$	J^{++}	1.08	0.91	0.89
	J^{x+}	1.23	0.96	0.82

* Time integration at 600 mb.

LIST OF FIGURES

Fig. 1. The numbering of the mesh points.

2. Error distribution of $\zeta^{x} - \zeta^{+}$.

3. Mesh points used in the calculations of Jacobians.

4. Mesh of 18 x 14 points.

5a 500 mb contours 1500Z 30.1.52.

5b 500 mb contours 1500Z 31.1.52.

5c Forecast 500 mb contours 1500Z 31.1.52 using J^{++}.

5d Forecast 500 mb contours 1500Z 31.1.52 using J^{x+}.

6a 500 mb contours 1500Z 27.1.52.

6b 500 mb contours 1500Z 28.1.52.

6c Forecast 500 mb contours 1500Z 28.1.52 using J^{++}.

6d Forecast 500 mb contours 1500Z 28.1.52 using J^{x+}.

7a 500 mb contours 1500Z 30.1.53.

7b 500 mb contours 1500Z 31.1.53.

7c Forecast 500 mb contours 1500Z 31.1.53 using J^{++}.

7d Forecast 500 mb contours 1500Z 31.1.53 using J^{x+}.

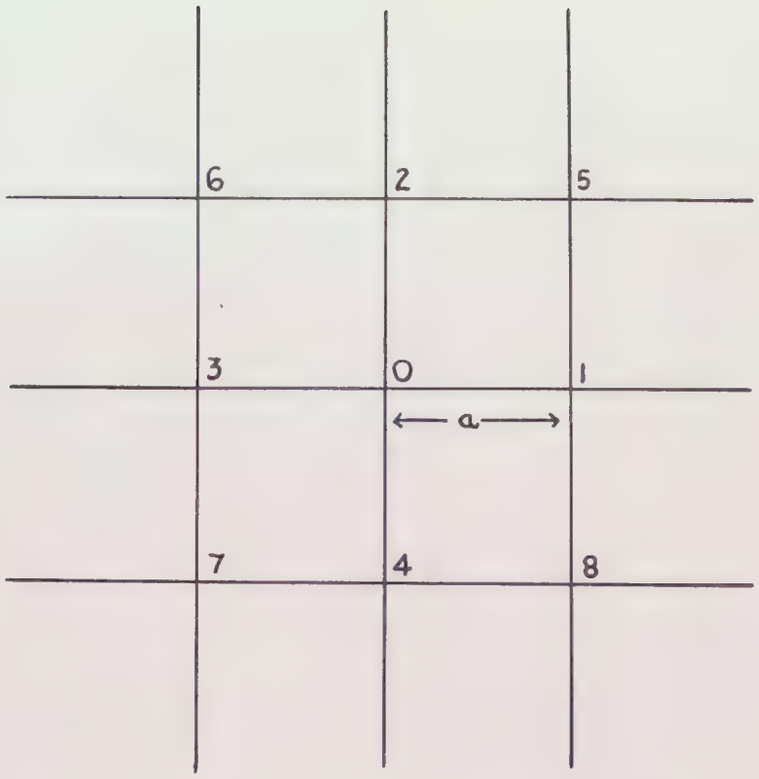

The numbering of the mesh points
Fig. 1

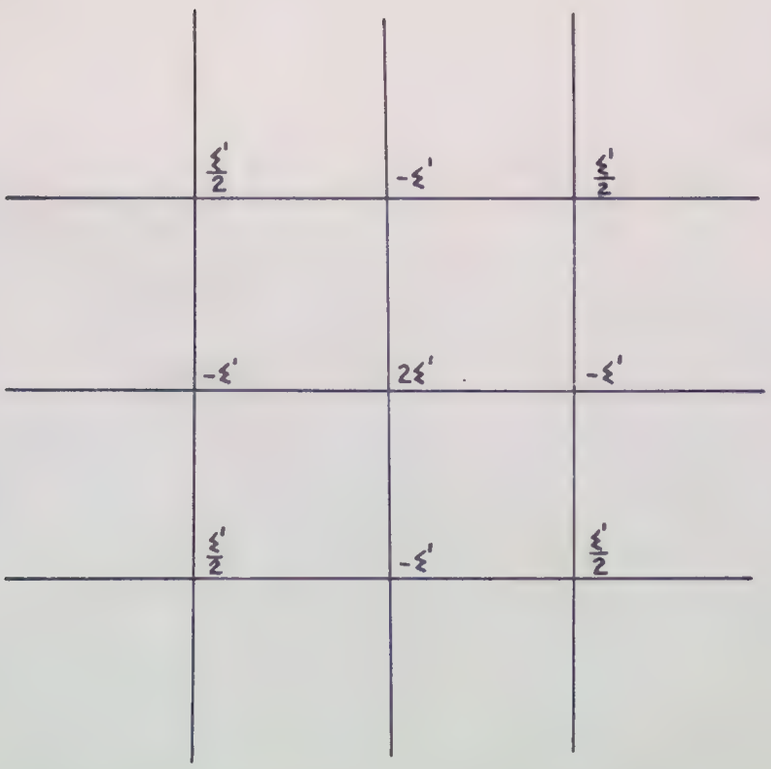

Error distribution of $S^x - S^+$
Fig. 2

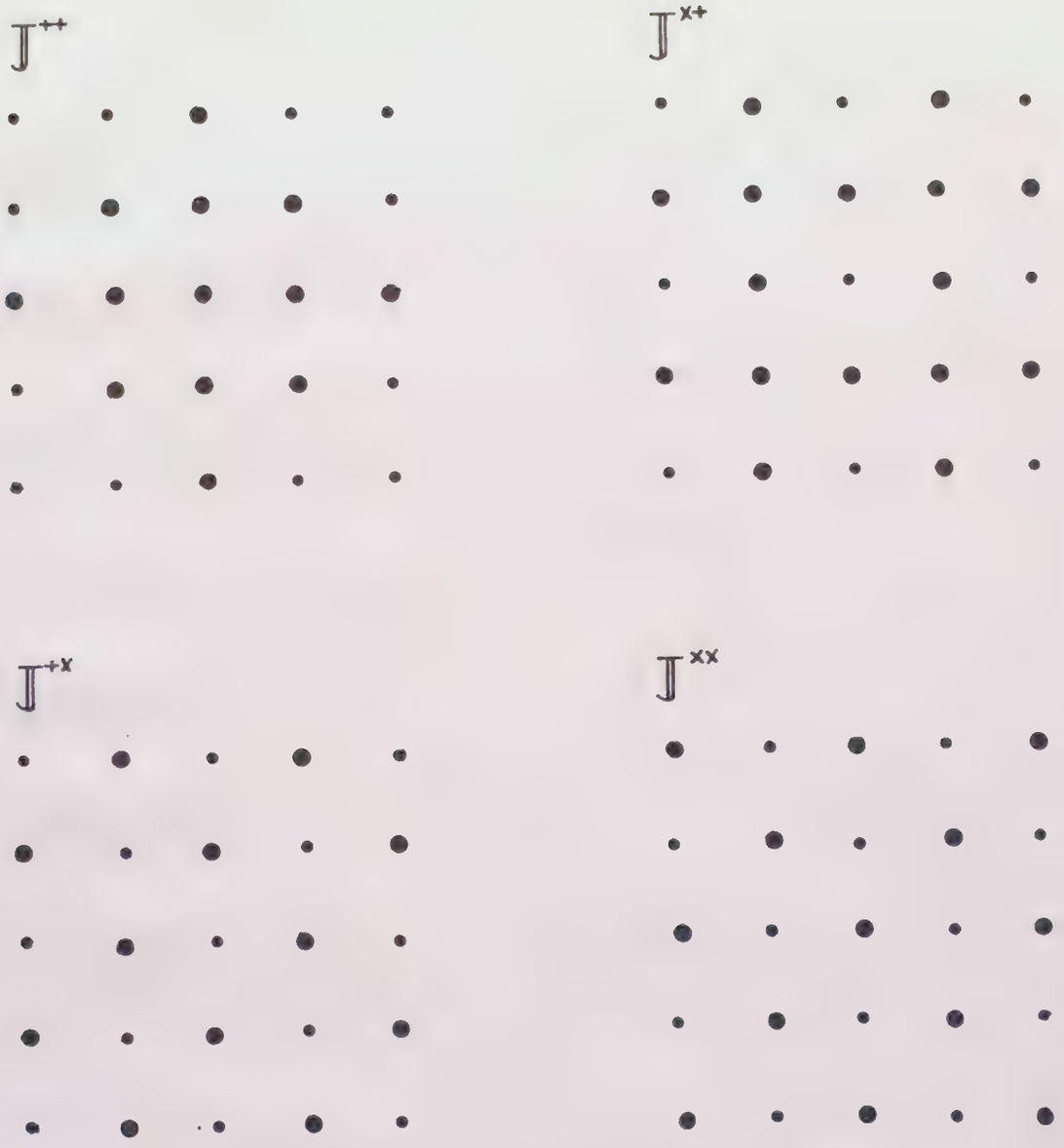

Mesh points used in the calculations of Jacobians

Fig. 3

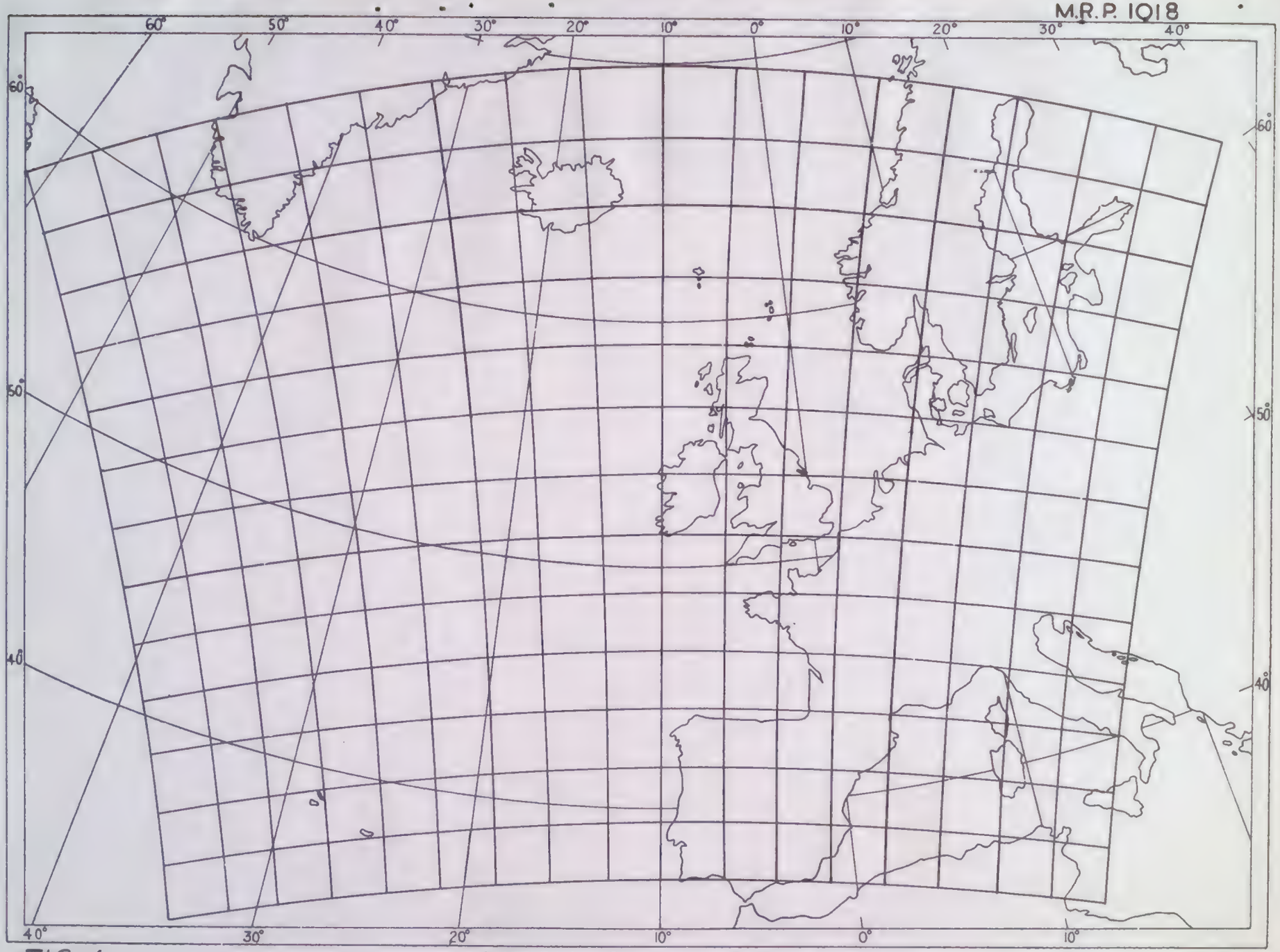

FIG. 4 MESH OF 18×14 POINTS

M.R.P. 1018

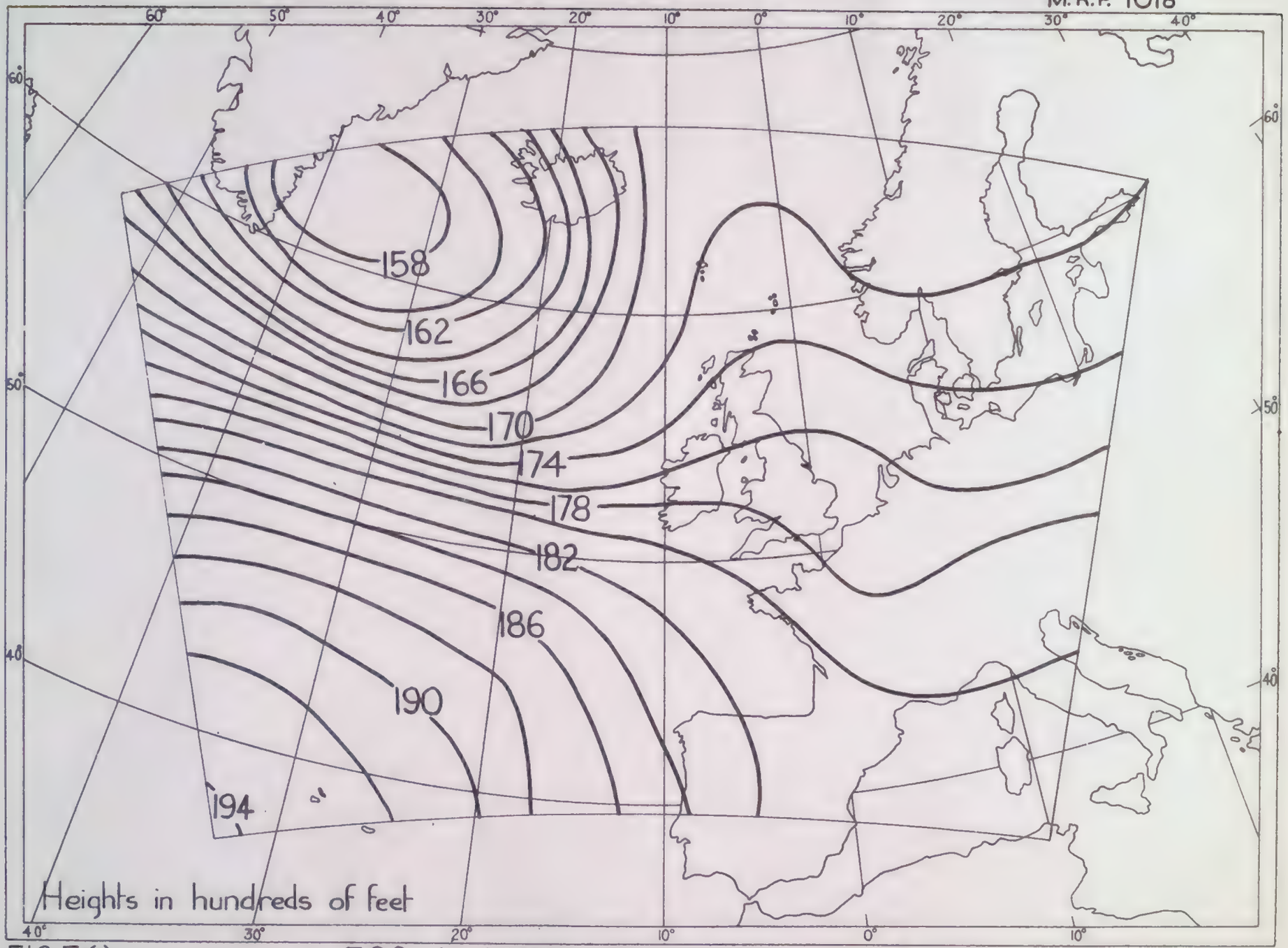

FIG.5(a) 500mb. CONTOURS 1500Z 30:1:52

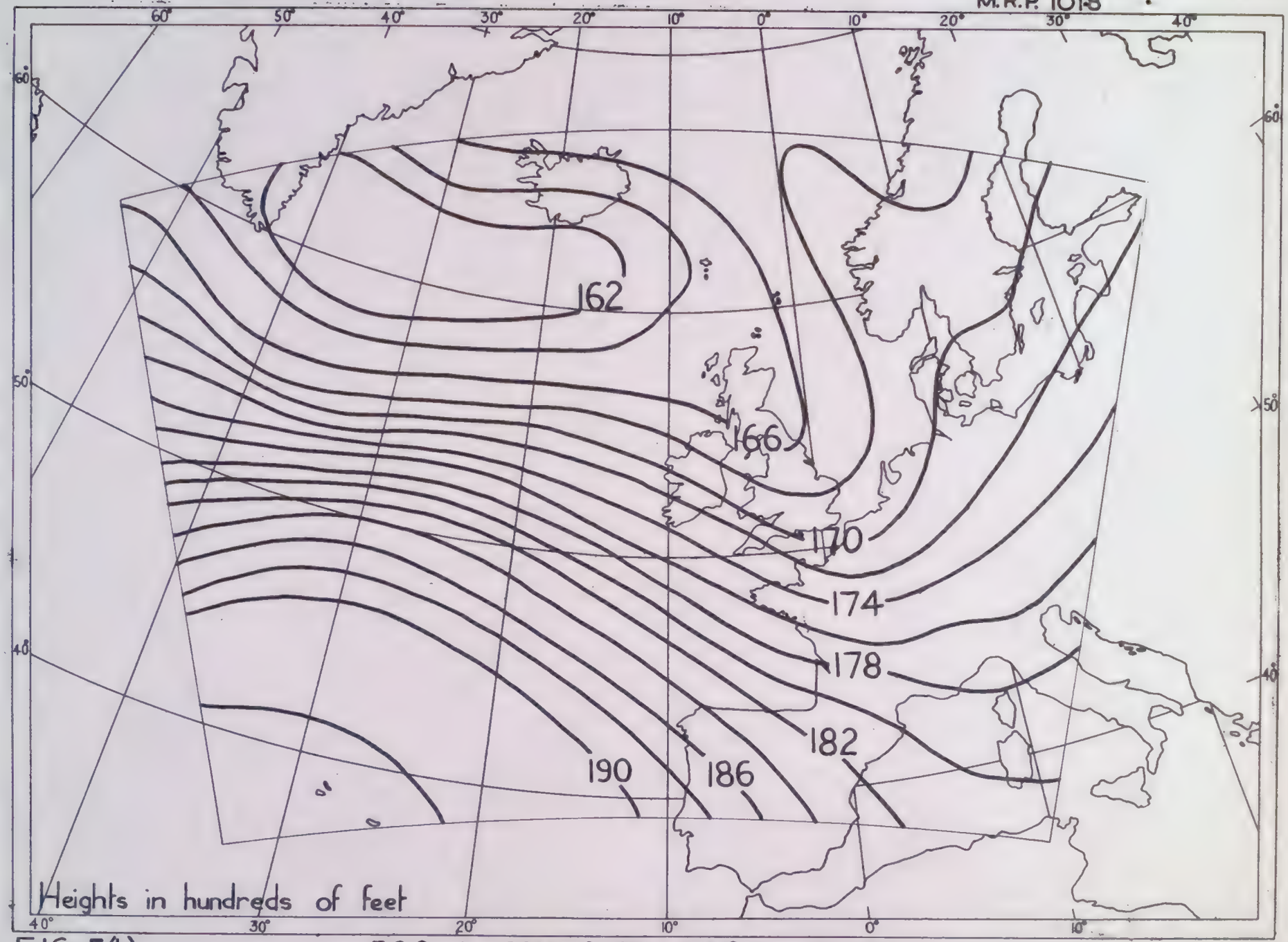

FIG. 5(b) 500mb. CONTOURS 1500Z 31:1:52

M.R.P. 1018

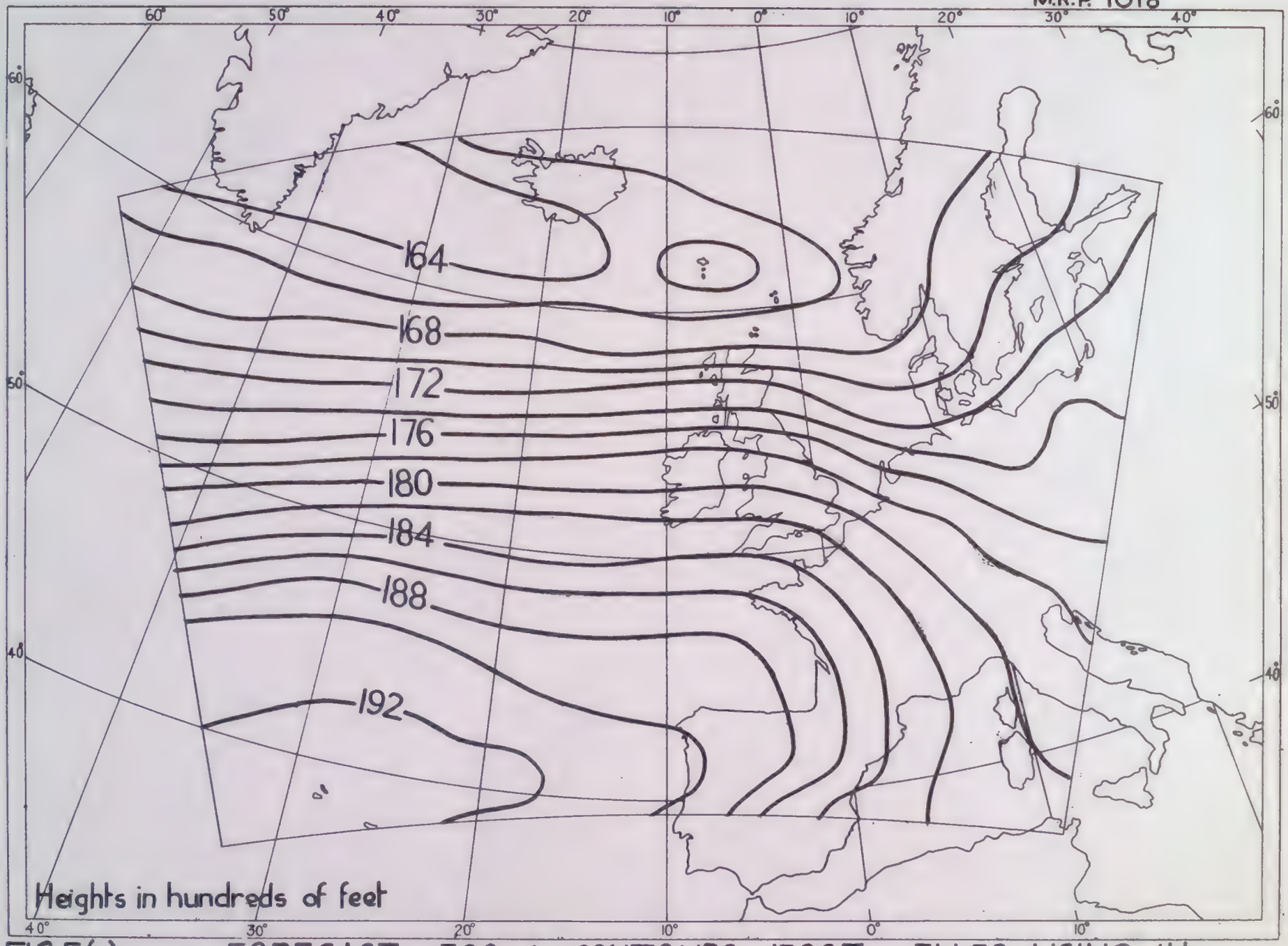

FIG.5(c) FORECAST 500mb. CONTOURS 1500Z 31:1:52 USING J++

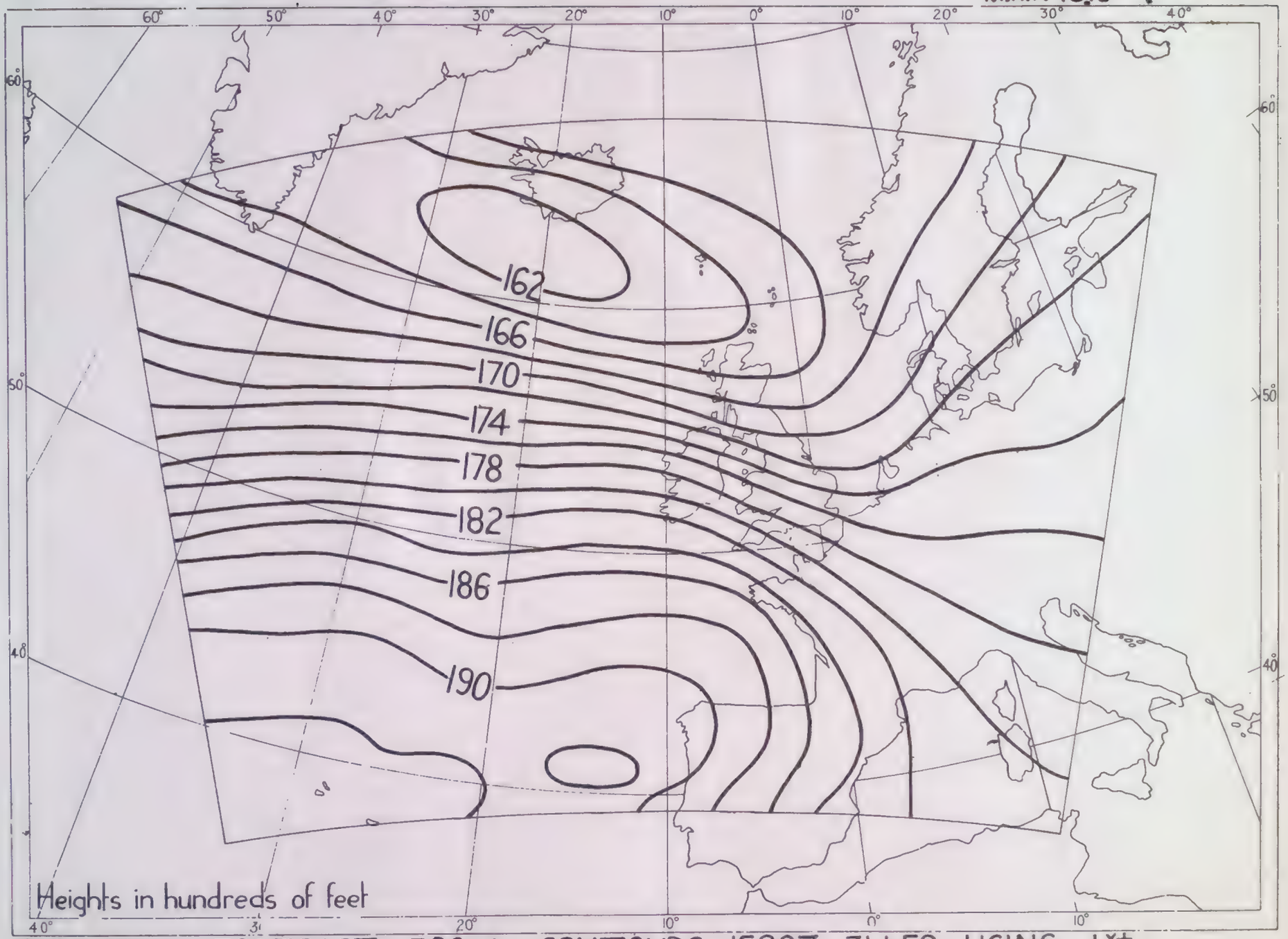

FIG.5(d) FORECAST 500mb. CONTOURS 1500Z 31:1:52 USING J^{x+}

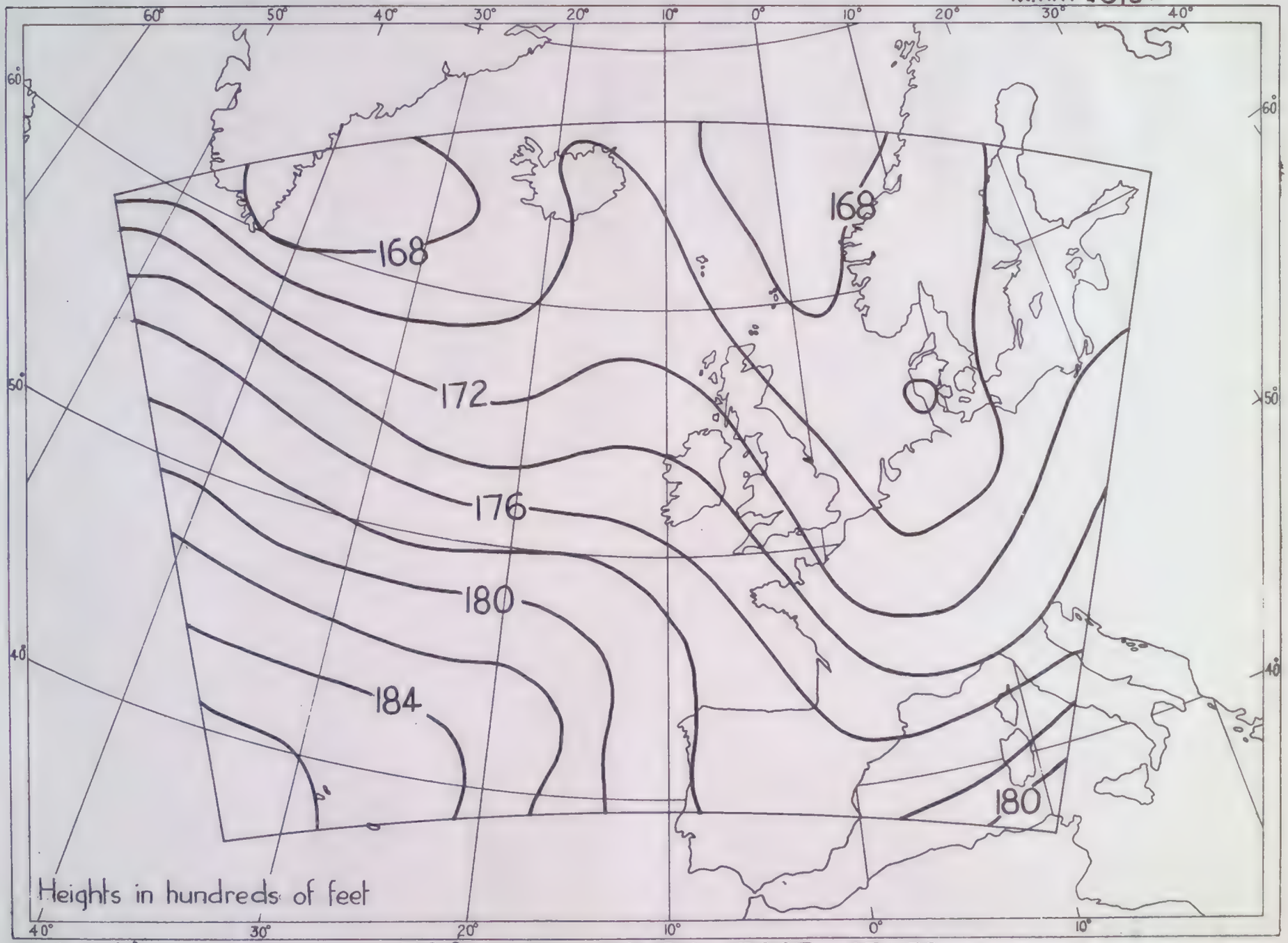

FIG. 6(a) 500mb. CONTOURS 1500Z 27:1:52

M.R.P. 1018

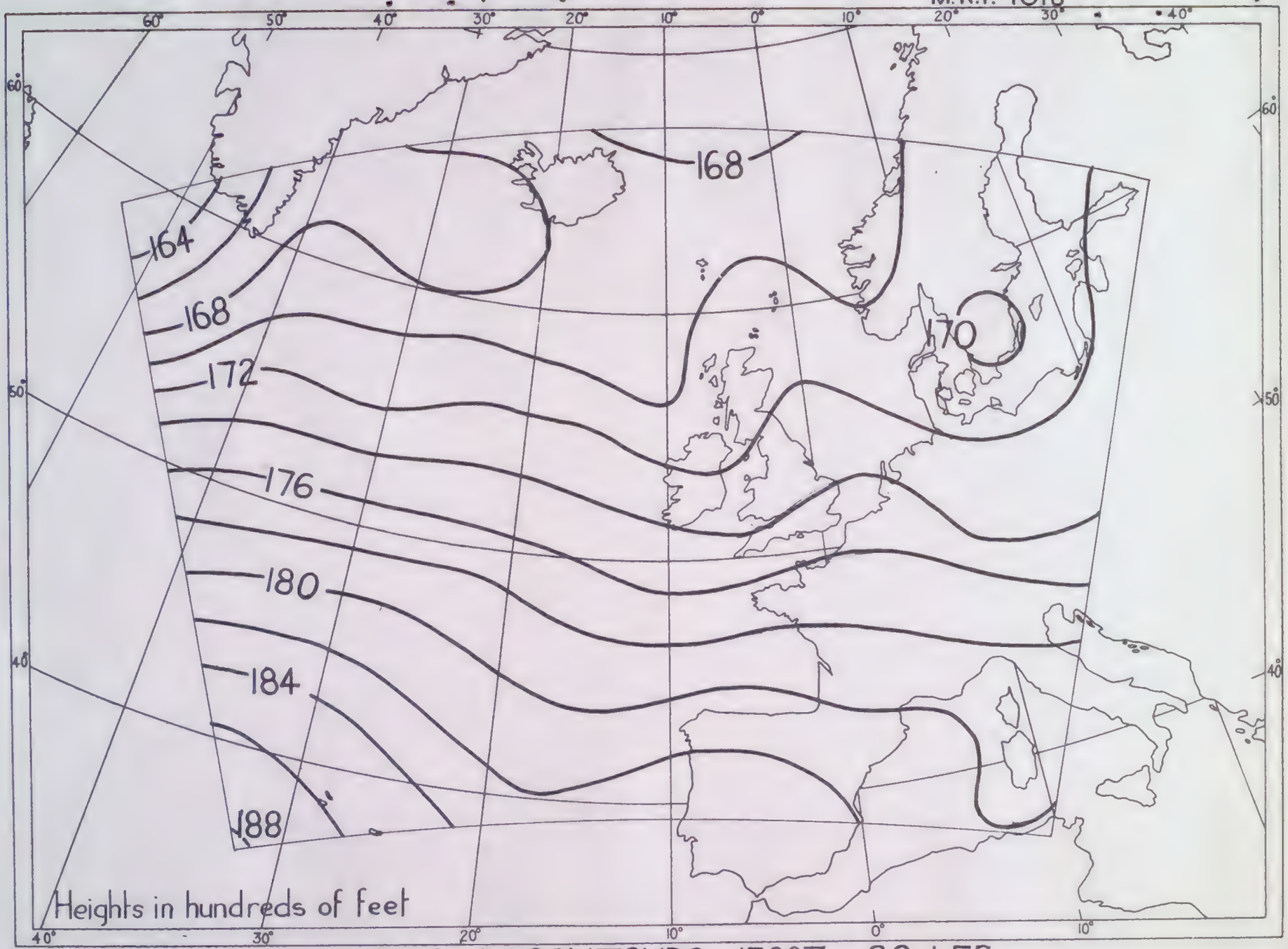

FIG. 6(b) 500 mb. CONTOURS 1500Z 28:1:52

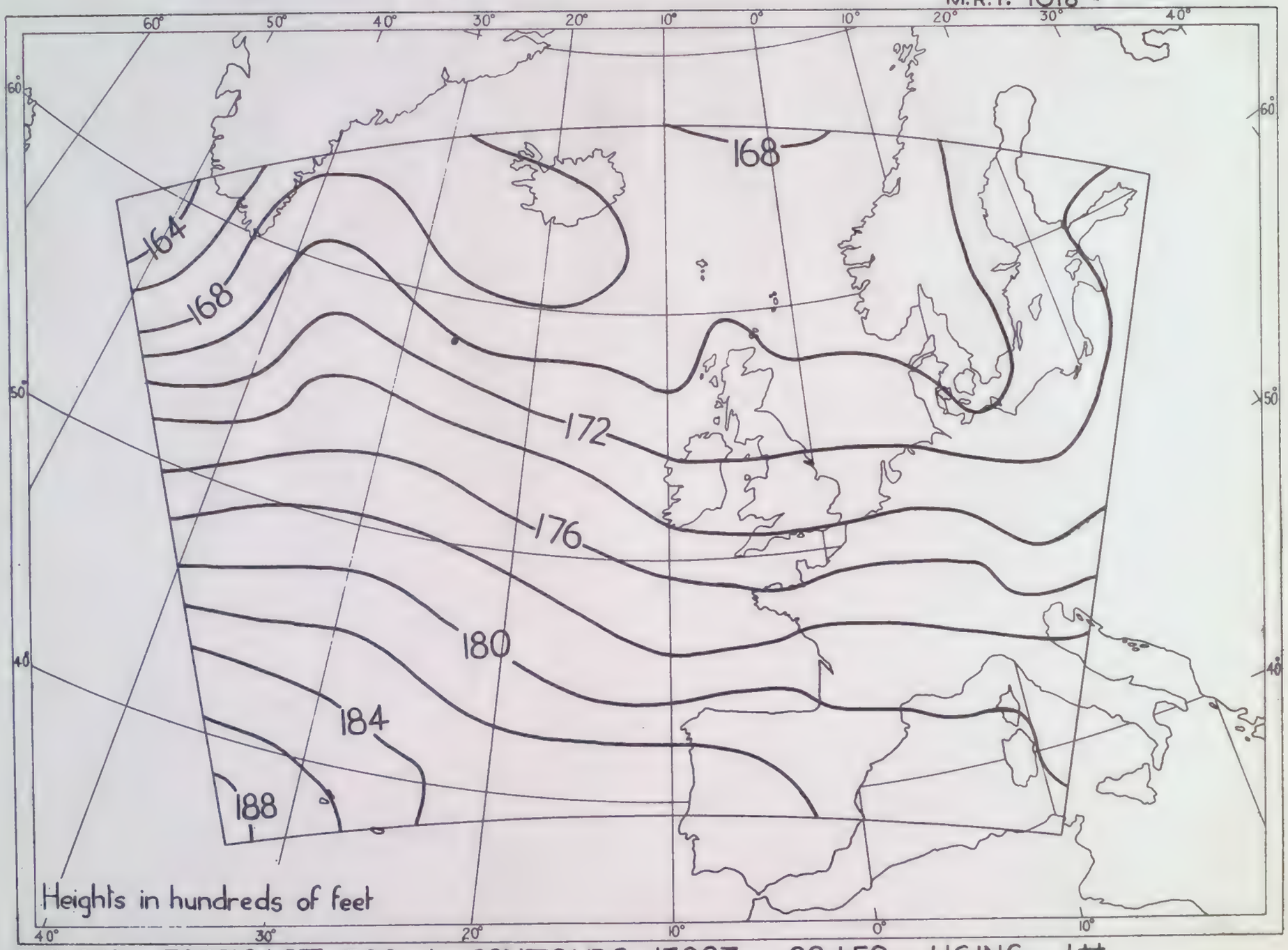

FIG. 6(c) FORECAST 500mb. CONTOURS 1500Z 28:1:52 USING J++

M.R.P. 1018

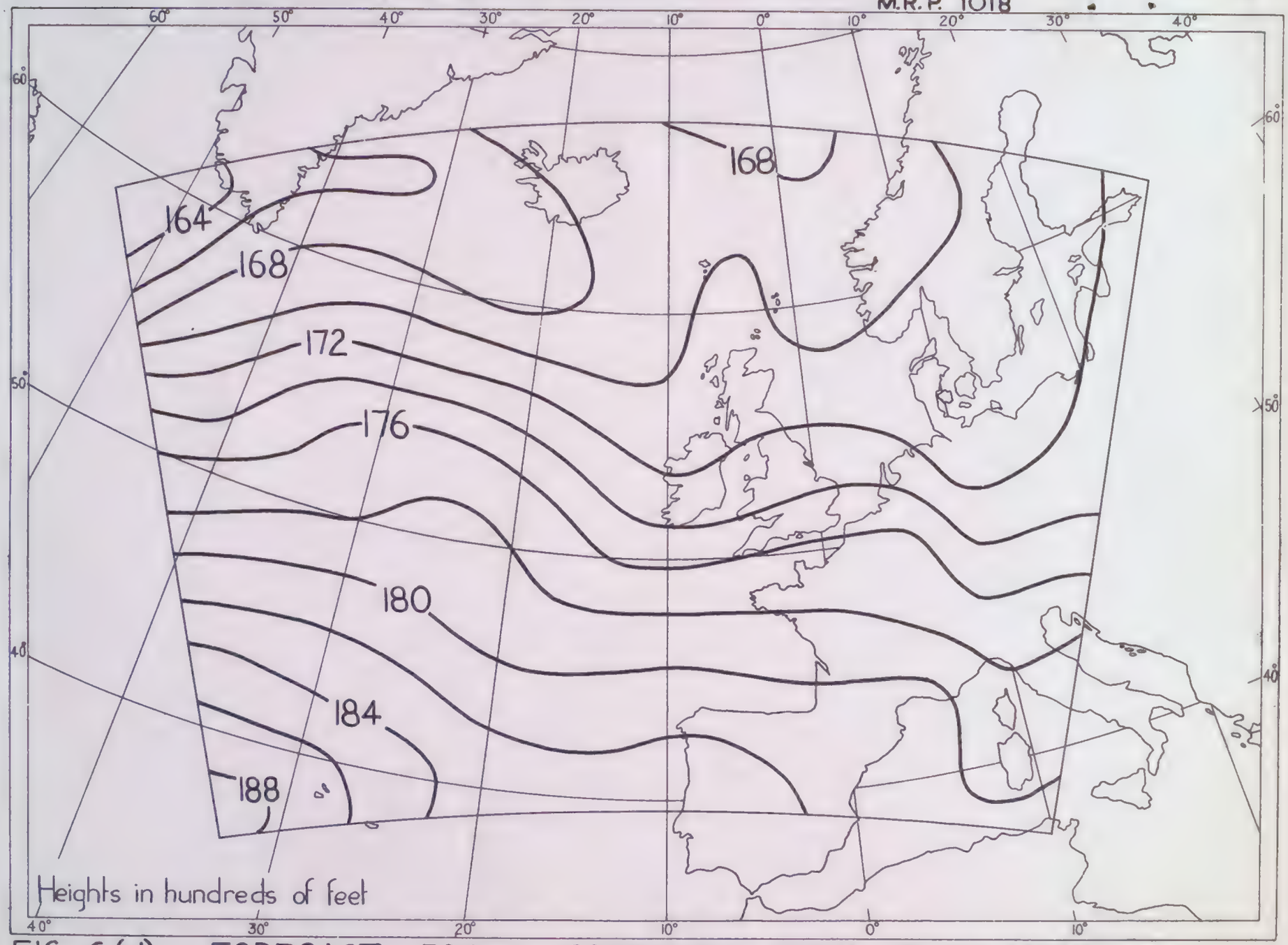

FIG. 6(d) FORECAST 500mb. CONTOURS 1500Z 28:1:52 USING J^x+

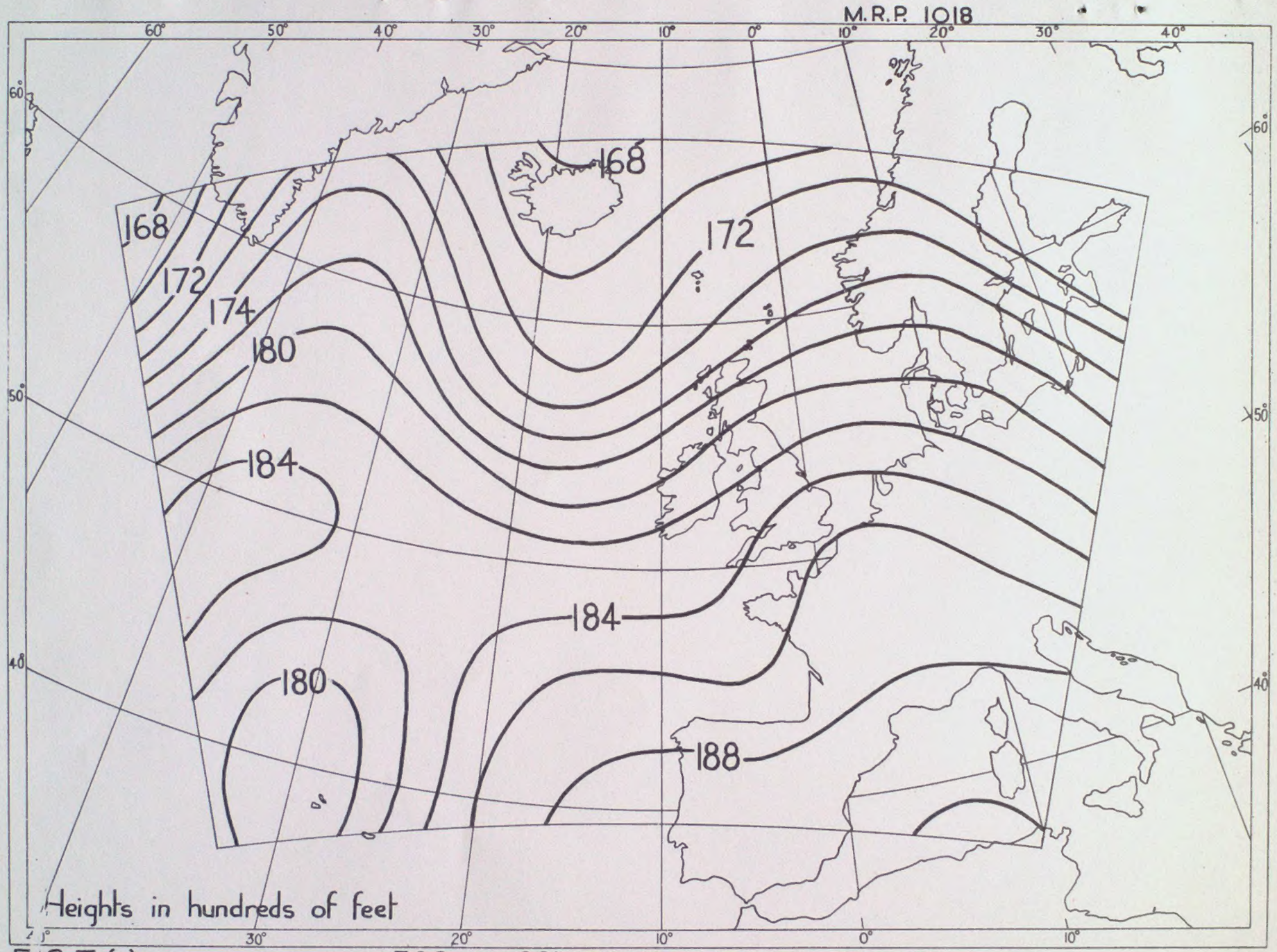

FIG. 7 (a) 500mb. CONTOURS 1500Z 30:1:53

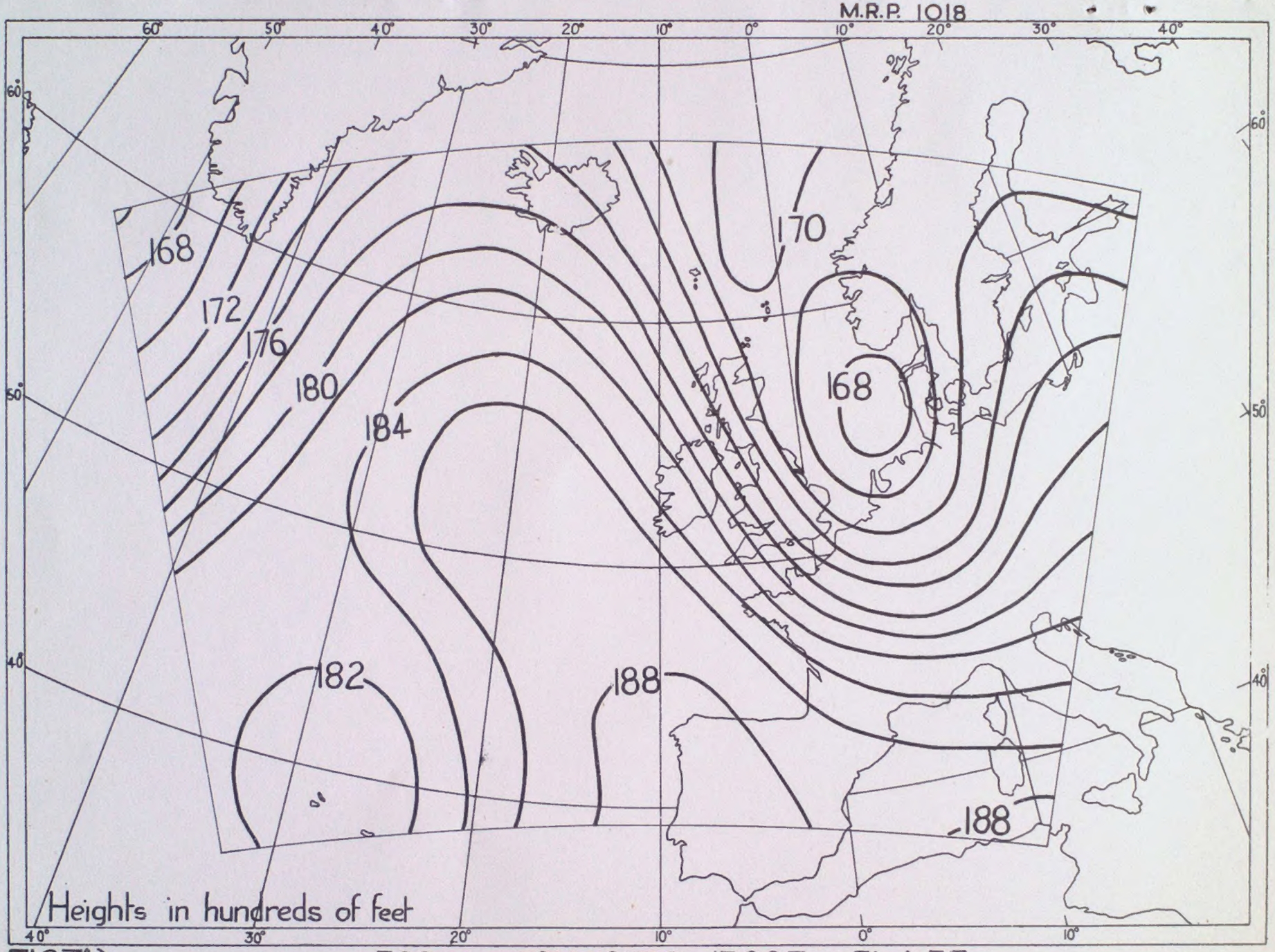

FIG.7(b) 500mb. CONTOURS 1500Z 31:1:53

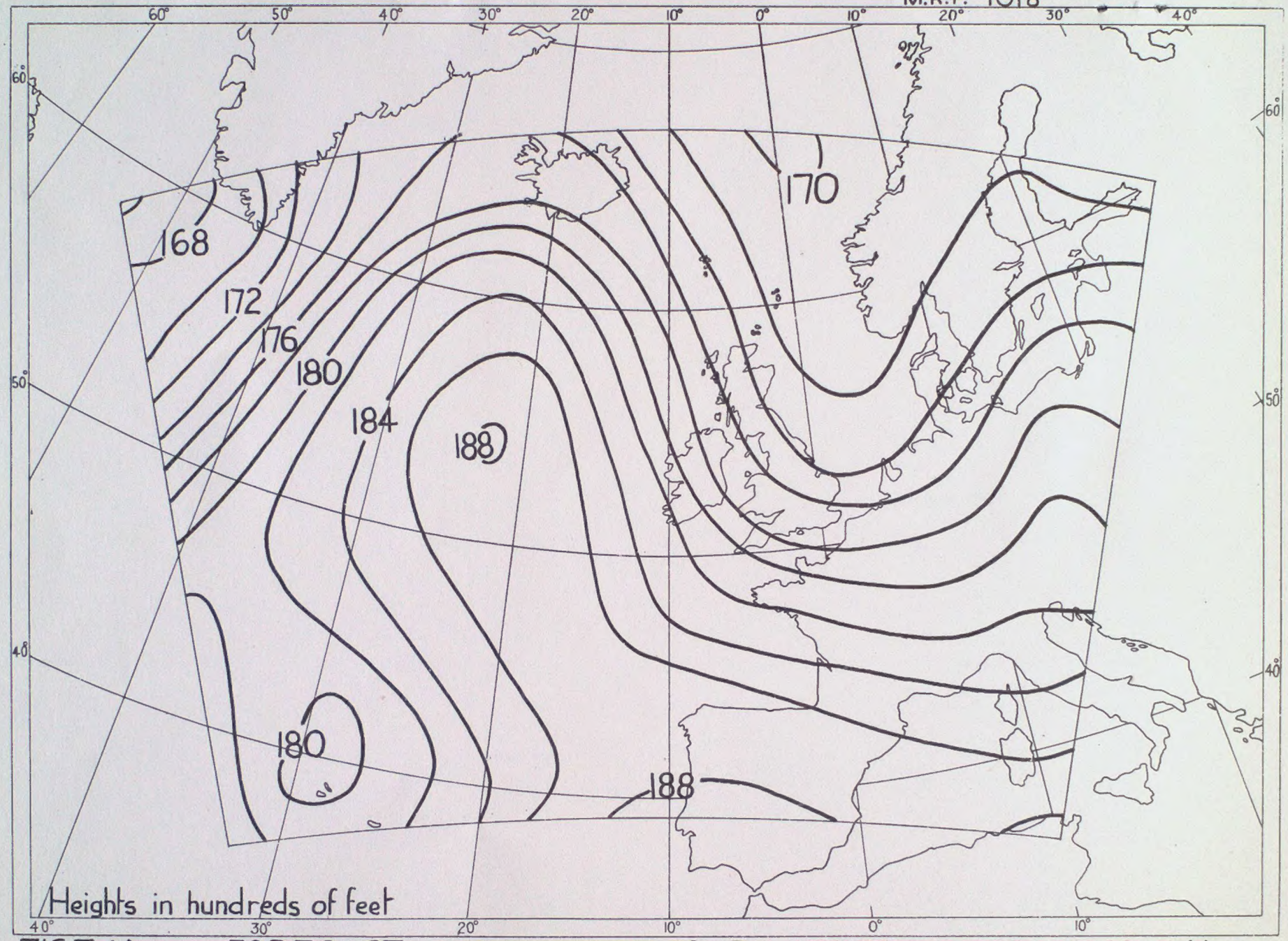

FIG.7 (c) FORECAST 500 mb. CONTOURS 1500Z 31:1:53 USING J++

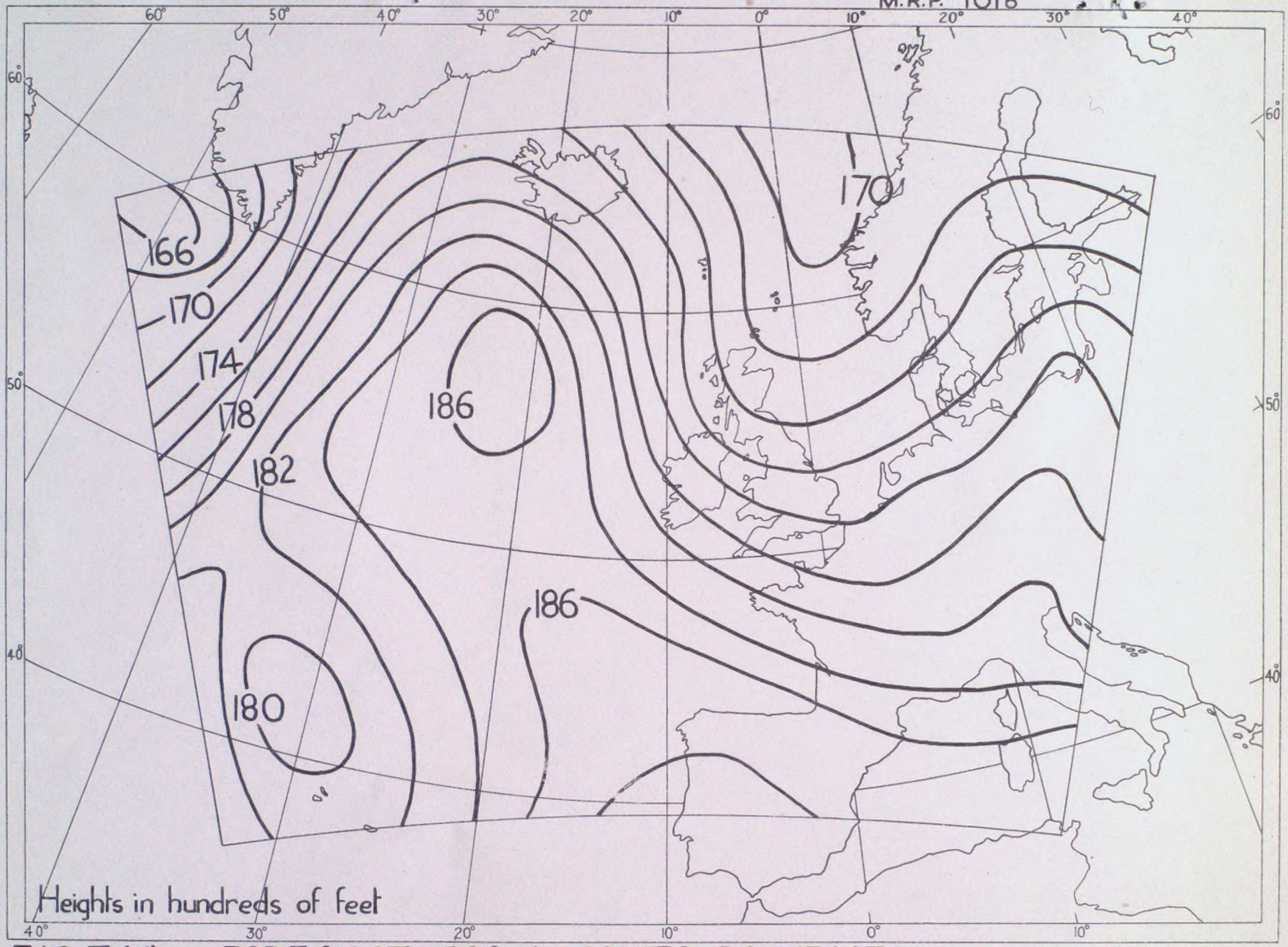

FIG. 7(d) FORECAST 500mb CONTOURS 1500Z 31:1:53 USING J^{x+}